Supplementary Information for

Understanding a Pentagonal-Bipyramidal Holmium(III) Complex with Record Energy Barrier for Magnetization Reversal

Yan Ma, Yuan-Qi Zhai, You-Song Ding, Tian Han* and Yan-Zhen Zheng*

[a] Frontier Institute of Science and Technology (FIST), School of Science, Shenzhen Research School, State Key Laboratory for Mechanical Behaviour of Materials, MOE Key Laboratory for Nonequilibrium Synthesis of Condensed Matter, Xi'an Key Laboratory of Sustainable Energy and Materials Chemistry,Xi'an Jiaotong University, 99 Yanxiang Road, Xi'an, Shaanxi 710054, P. R. China.

Corresponding email: hantian0123@xjtu.edu.cn; zheng.yanzhen@xjtu.edu.cn.

Contents

Experimental Details

1. Materials

All reactions were carried out under a dry and oxygen-free argon atmosphere in a glovebox. THF, hexane and pyridine were dried and degassed by standard techniques. Anhydrous $HoCl_3$ salts were prepared according to literature procedures. $NaOSiMe_3$, 3,5-Dimethylphenol, (R)-(+)-1-Phenylethanol and $NaBPh_4$ are commercially available and were used without further treatment.

2. Synthesis of compounds.

Synthesis of $[Ho(OSiMe_3)_2(py)_5][BPh_4]$ (1). $HoCl_3$ (0.5 mmol, 0.135 g), $NaOSiMe_3$ (1 mmol, 0.112 g) and $NaBPh_4$ (0.5 mmol, 0.171 g) were combined in 8mL THF gives a cloudy solution, which was filtered and then the solvent was removed under vacuum to give a white powder. The powder dissolved in 2 mL pyridine and then layered with 8 mL of hexane and stored at −35 °C, which gave pale-yellow crystals of **1** (yield ca. 40 %). Elemental analysis/%, found (calculated) for **1**： C 53.35(52.59); H 5.80(5.14); N 5.61(5.45). The diluted sample was synthesized in the same way, with the starting $HoCl_3$:YCl_3=1:9. A 100 mg sample of Compound **1** was completely dissolved in 1 ml of pyridine to make a solution sample.

Synthesis of $[Y(OSiMe_3)_2(py)_5][BPh_4]$ (1Y). The synthesis was the same as **1** with $HoCl_3$ replaced by YCl_3. The pyridine solution was layered with 8mL of hexane and stored at −35 °C, which gave colorless crystals of **1Y** (yield ca. 55 %).

Synthesis of $[Ho(OCH(CH_3)C_6H_5)_2(py)_5][BPh_4]$ (2). The synthesis was the same as **1** with $NaOSiMe_3$ replaced by 1 mmol of $NaOCH(CH_3)C_6H_5$. The pyridine solution was layered with 8mL of hexane and stored at −35 °C, which gave pale-yellow crystals of **2**. Elemental analysis/%, found (calculated) for **2**： C 66.27 (66.34); H 6.07(5.68); N 5.94(5.70).

Synthesis of $[Ho(OC_6H_3(CH_3)_2)_2(py)_5][BPh_4]$ (3). The synthesis was the same as **1** with NaOSiMe3 replaced by 1 mmol of $NaOC_6H_3(CH_3)_2$. The pyridine solution was layered with 8 mL of hexane and stored at −35 °C, which gave pale-yellow crystals of **3**. Elemental analysis/%, found (calculated) for **3**： C 69.58 (66.87); H 5.66(5.85); N 6.24(6.54).

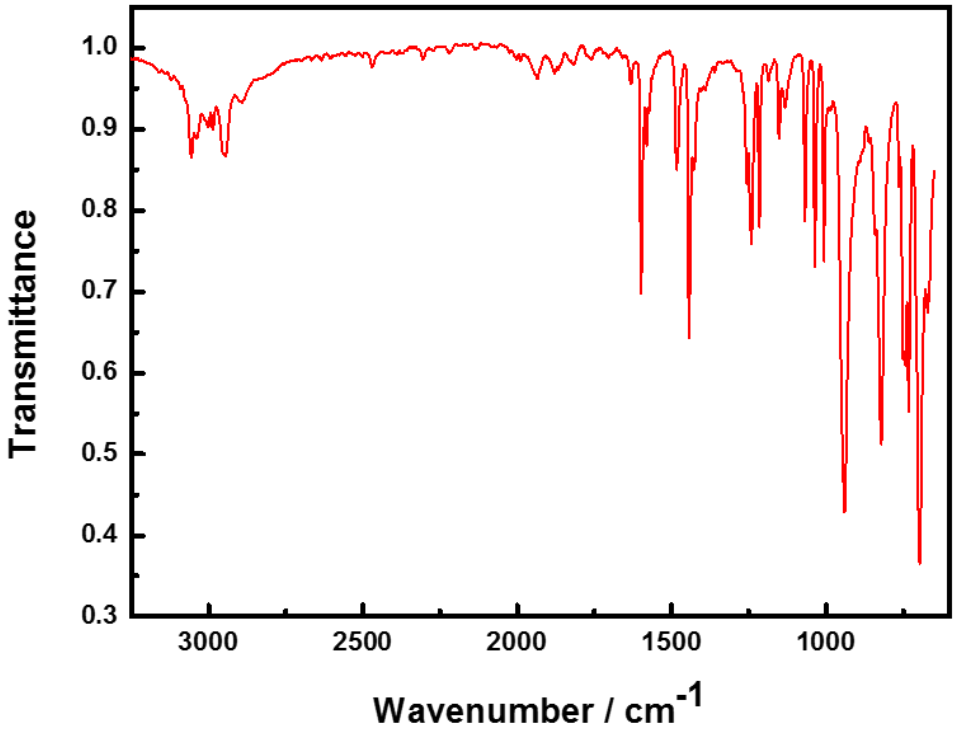

Fig. S1. IR spectra of solid **1**.

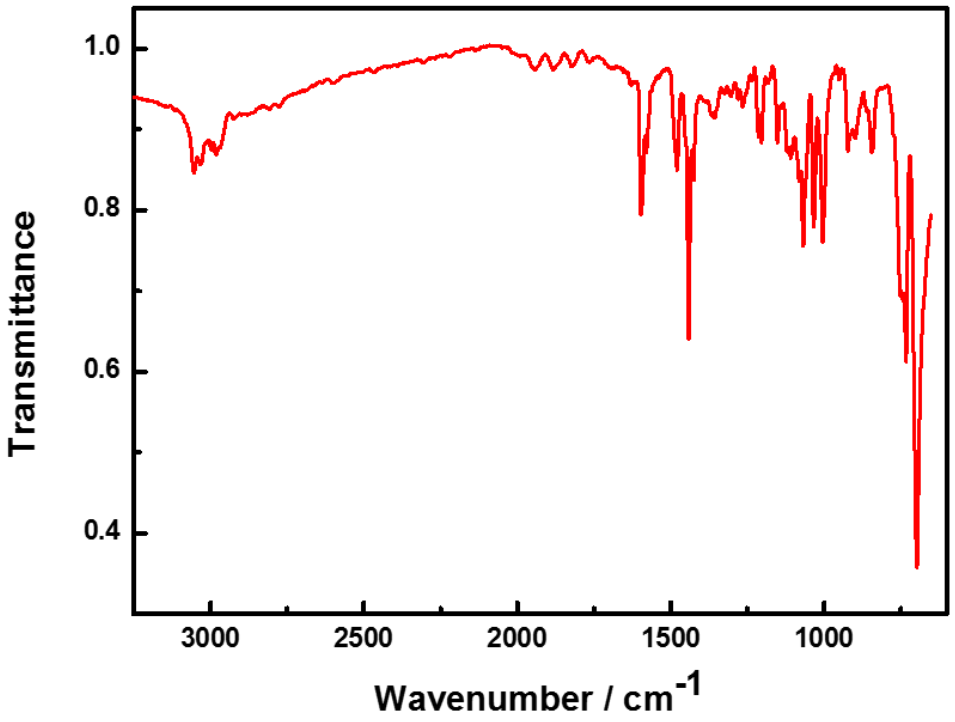

Fig. S2. IR spectra of solid **2**.

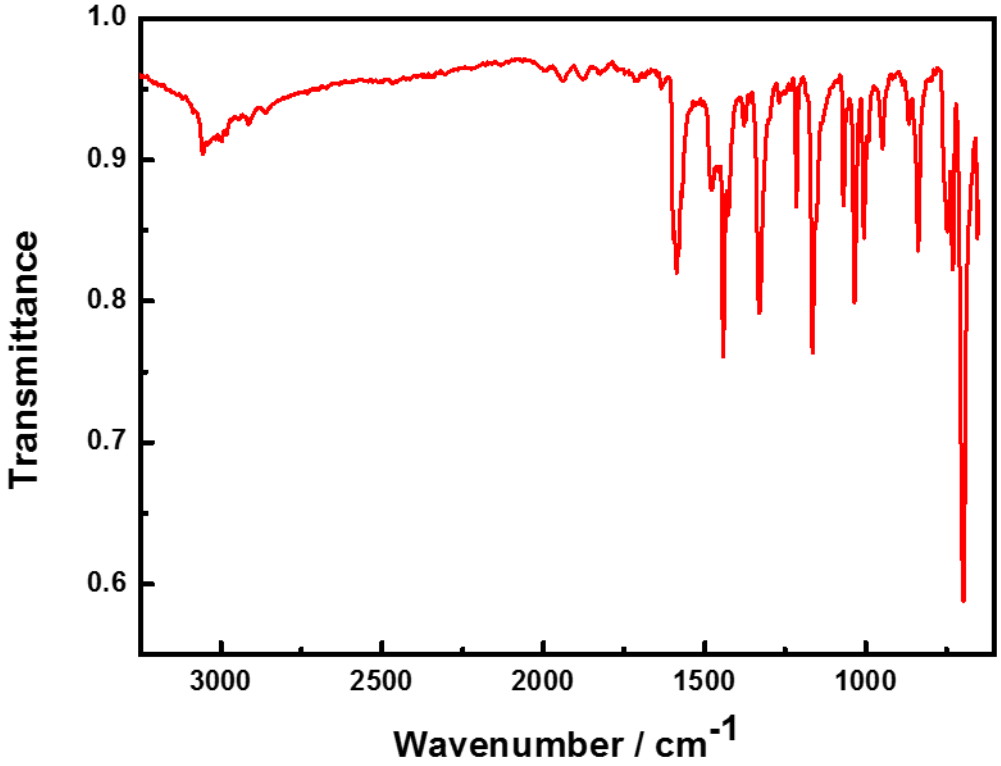

Fig. S3. IR spectra of solid **3**.

3. Crystal Data and Structures

All data were recorded on a Bruker SMART CCD diffractometer with MoKα radiation (λ = 0.71073 Å). The structures were solved by direct methods and refined on F^2 using SHELXTL. Crystal data for the structures reported in this paper have been deposited in the Cambridge Crystallographic Database Center： CCDC 1962740(**1Y**), 1962742(**1**), 1962743(**2**), 1962868(**3**).

Table S1. Comparison of selected structural parameters for **1**, **2**, **3** and $[Ho(CyPh_2PO)_2(H_2O)_5]I_3$.. (bond lengths (Å) and angles (deg)).

	1	**2**	**3**		$[Ho(CyPh_2PO)_2(H_2O)_5]I_3$
Ho1-O1	2.1395(18)	2.117(3)	2.144(4)	Ho1-O1	2.198(6)
Ho1-O2	2.1390(18)	2.112(3)	2.138(4)	Ho1-O1A	2.198(6)
Ho1-N1	2.547(2)	2.548(4)	2.548(6)	Ho1-O1W	2.323(7)
Ho1-N2	2.520(2)	2.532(4)	2.563(6)	Ho1-O2W	2.350(7)
Ho1-N5	2.557(2)	2.564(4)	2.553(6)	Ho1-O2WA	2.350(7)
Ho1-N4	2.541(2)	2.545(4)	2.525(6)	Ho1-O3W	2.349(7)
Ho1-N3	2.530(2)	2.533(4)	2.579(7)	Ho1-O3WA	2.349(7)
Ho-N(average)	2.539	2.5444	2.5536	Ho-OW(average)	2.3442
O2-Ho1-O1	176.12(7)	174.51(14)	175.68(18)	O1–Ho–O1A	177.9(4)
N4-Ho1-N5	71.15(7)	74.58(13)	71.97(18)	O1W–Ho–O2W	71.53(17)
N2-Ho1-N1	72.93(8)	72.77(13)	70.7(2)	O2W–Ho–O3W	72.4(2)
N2-Ho1-N3	71.89(8)	74.77(13)	73.7(2)	O3W–Ho–O3WA	72.5(4)
N3-Ho1-N4	72.09(8)	69.20(13)	72.80(19)	O3WA–Ho–O2WA	72.4(2)
N2-Ho1-N3	71.89(8)	68.71(13)	71.91(18)	O2WA–Ho–O1W	71.53(17)
N-Ho-N(average)	71.99	72.006	72.216	OW–Ho–OW(average)	72.072
CShM PBPY-7(D_{5h})	0.754	0.778	0.881	CShM PBPY-7(D_{5h})	0.160
Ho···Ho	9.8860	10.5803	11.1588	Ho···Ho	14.08
ρ_{calc}[g/cm^3]	1.303	1.332	1.240	ρ_{calc}[g/cm^3]	1.447

Table S2. Selected bond lengths (Å) and angles (deg) in **1Y** and **1@1Y**.

1@1Y		**1Y**	
Y(Ho)1-O1	2.147(2)	Y1-O1	2.1499(15)
Y(Ho)1-O2	2.128(3)	Y1-O2	2.1350(16)
Y(Ho)1-N1	2.554(3)	Y1-N1	2.5436(19)
Y(Ho)1-N2	2.565(3)	Y1-N2	2.527(2)
Y(Ho)1-N5	2.532(3)	Y1-N5	2.568(2)
Y(Ho)1-N4	2.527(3)	Y1-N4	2.544(2)
Y(Ho)1-N3	2.543(3)	Y1-N3	2.5295(19)
O2-Y(Ho)1-O1	176.01(9)	O2-Y1-O1	176.03(6)
O1-Y(Ho)1-N1	87.78(11)	O1-Y1-N1	89.60(6)
O1-Y(Ho)1-N4	87.76(11)	O1-Y1-N4	91.74(6)
O1-Y(Ho)1-N2	90.65(10)	O1-Y1-N2	88.75(7)
O1-Y(Ho)1-N3	91.76(10)	O1-Y1-N3	88.55(6)
O1-Y(Ho)1-N5	89.50(11)	O1-Y1-N5	95.76(7)
O2-Y(Ho)1-N1	88.25(11)	O2-Y1-N1	88.84(6)
O2-Y(Ho)1-N4	95.32(11)	O2-Y1-N4	91.72(6)
O2-Y(Ho)1-N2	88.59(11)	O2-Y1-N2	90.53(6)
O2-Y(Ho)1-N3	91.69(10)	O2-Y1-N3	87.51(6)
O2-Y(Ho)1-N5	88.98(11)	O2-Y1-N5	87.26(6)
N4-Y(Ho)1-N5	72.8911)	N4-Y1-N5	69.99(6)
N2-Y(Ho)1-N1	73.35(10)	N2-Y1-N1	73.18(6)
N2-Y(Ho)1-N3	70.84(10)	N2-Y1-N3	70.99(6)
N3-Y(Ho)1-N4	69.77(10)	N3-Y1-N4	72.61(6)
N1-Y(Ho)1-N5	73.27(11)	N1-Y1-N5	73.33(6)

Table S3. Crystal data and structure refinement for **1**, **1@1Y** and **1Y**. *continued*

Compound	**1**	**1@1Y**	**1Y**
Formula	$HoC_{67}H_{75}BN_8O_2Si_2$	$Ho_{0.12}Y_{0.88}C_{55}H_{63}BN_5O_2Si_2$	$YC_{55}H_{63}BN_5O_2Si_2$
M, g mol^{-1}	1256.27	990.93	982.00
T(K)	150	150	150
Crystal system	triclinic	monoclinic	monoclinic
Space group	P-1	$P2_1/c$	$P2_1/c$
a[Å]	13.665(2)	12.097(7)	12.054(5)
b[Å]	14.335(2)	22.399(12)	22.253(8)
c[Å]	17.329(3)	20.475(11)	20.280(8)
α[°]	95.521(2)	90	90
β[°]	108.465(2)	93.864(8)	93.554(5)
γ[°]	90.850(2)	90	90
V[Å^3]	3201.2(9)	5535(5)	5429(4)
Z	2	4	4
ρ_{calc}[g/cm^3]	1.303	1.189	1.201
Reflections collected	29507	36073	52752
Independent reflections	13311 [R_{int} = 0.0230, R_{sigma} = 0.0326]	10136 [R_{int} = 0.0651, R_{sigma} = 0.0739]	9878 [R_{int} = 0.0448, R_{sigma} = 0.0347]
Data/restraints/parameters	13311/50/736	10136/12/602	9878/0/601
Goodness-of-fit on F^2	1.029	1.000	1.028
Final R indexes [I>=2σ (I)]	R_1= 0.0314, wR_2 = 0.0751	R_1 = 0.0460, wR_2 = 0.0995	R_1 = 0.0339, wR_2 = 0.0752
Final R indexes [all data]	R_1= 0.0367, wR_2 = 0.0779	R_1 = 0.1085, wR_2 = 0.1252	R_1 = 0.0557, wR_2 = 0.0841
Largest diff. peak/hole / e Å^{-3}	1.75/-0.80	0.64/-0.54	0.31/-0.34

Table S3. Crystal data and structure refinement for **2** and **3**.

Compound	**2**	**3**
Formula	$C_{70}H_{68}BHoN_6O_2$	$C_{70}H_{74}BHoN_8O_2$
M, g mol^{-1}	1201.04	5117.57
T(K)	150	150.0
Crystal system	orthorhombic	triclinic
Space group	$P2_12_12$	P-1
a[Å]	21.104(8)	15.645(11)
b[Å]	25.522(9)	15.651(11)
c[Å]	11.123(4)	28.55(2)
α[°]	90	101.047(9)
β[°]	90	93.207(9)
γ[°]	90	90.009(9)
V[Å^3]	5991(4)	6851(8)
Z	4	1
ρ_{calc}[g/cm^3]	1.332	1.240
Reflections collected	58226	68037
Independent reflections	11108 [R_{int} = 0.0495, R_{sigma} =	25855 [R_{int} = 0.0486, R_{sigma} =
Data/restraints/parameters	11108/0/723	25855/144/1597
Goodness-of-fit on F^2	1.049	1.057
Final R indexes [I>=2σ (I)]	R_1 = 0.0286, wR_2 = 0.0596	R_1 = 0.0634, wR_2 = 0.1531
Final R indexes [all data]	R_1 = 0.0340, wR_2 = 0.0615	R_1 = 0.0816, wR_2 = 0.1622
Largest diff. peak/hole / e Å^{-3}	0.97/-0.50	2.02/-3.15

Table S4. Continuous Shape Measures calculations(CShM).

Complex	HP-7 (D_{7h})	HPY-7 (C_{6V})	PBPY-7 (D_{5h})	COC-7 (C_{3V})	CTPR-7 (C_{3V})	JPBPY-7 (D_{5h})	JETPY-7 (C_{3V})
1	33.685	24.000	0.754	7.435	5.640	1.571	22.810
1@1Y	32.799	23.871	0.675	7.972	6.041	1.438	23.423
1Y	32.783	23.941	0.659	7.960	5.987	1.466	23.386
2	32.310	23.301	0778	8.066	6.409	1.390	23.463
3	33.247	23.847	0.881	6.847	4.948	1.625	22.592

HP-7 = Heptagon; HPY-7 = Hexagonal pyramid; PBPY-7 = Pentagonal bipyramid; COC-7 = Capped octahedron; CTPR-7 =Capped trigonal prism; JPBPY-7 = Johnson pentagonal bipyramid J13; JETPY-7 = Johnson elongated triangular pyramid J7.

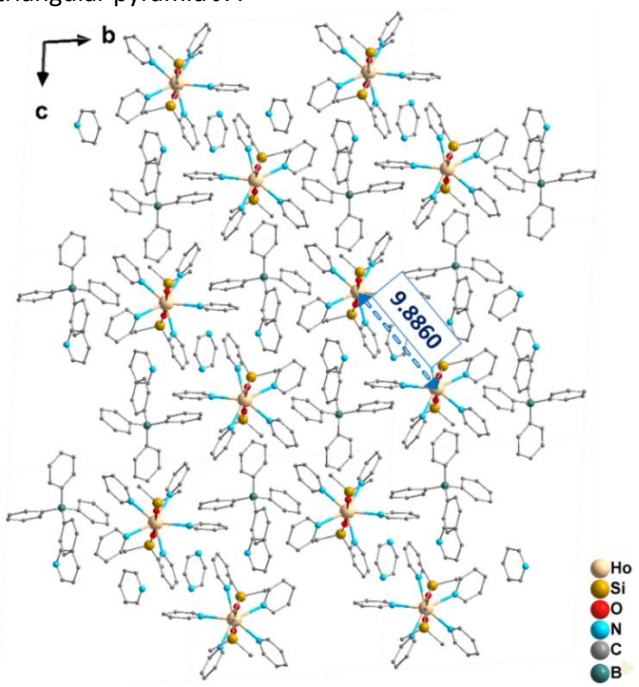

Fig. S4. Packing of **1** in the crystal structure viewed along the *a* axis. H atoms are omitted for clarity.

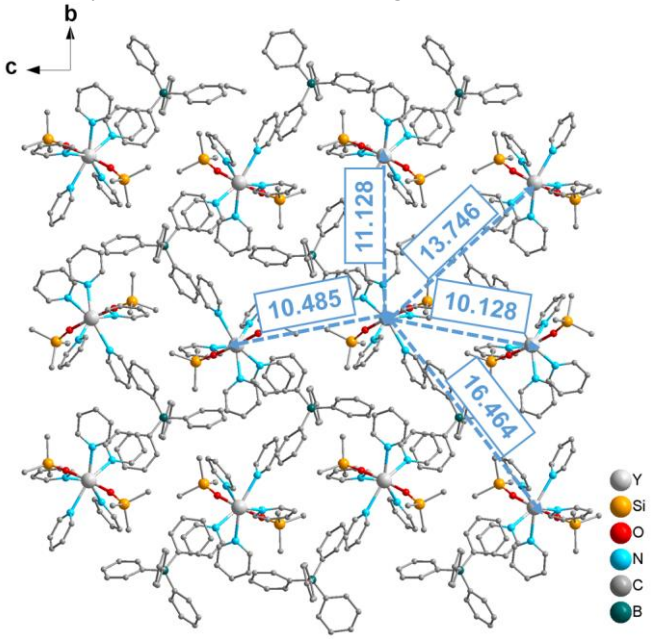

Fig. S5. Packing of **1Y** in the crystal structure viewed along the *a* axis. H atoms are omitted for clarity.

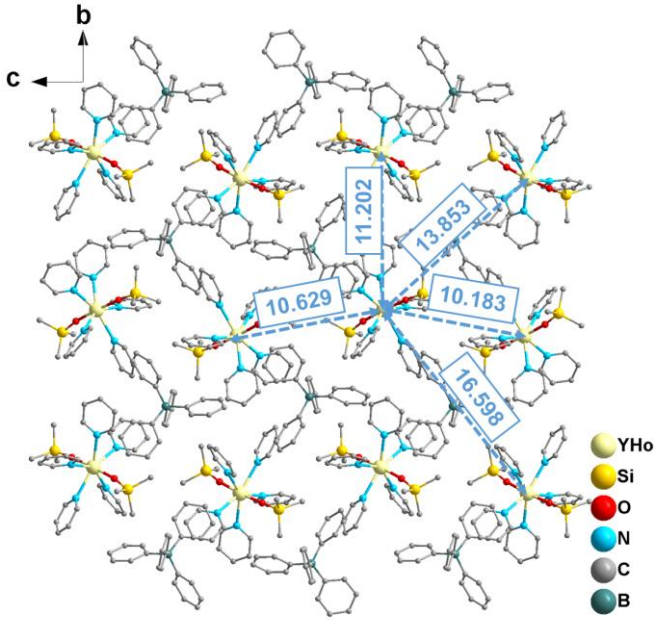

Fig. S6. Packing of **1@1Y** in the crystal structure viewed along the *a* axis. H atoms are omitted for clarity.

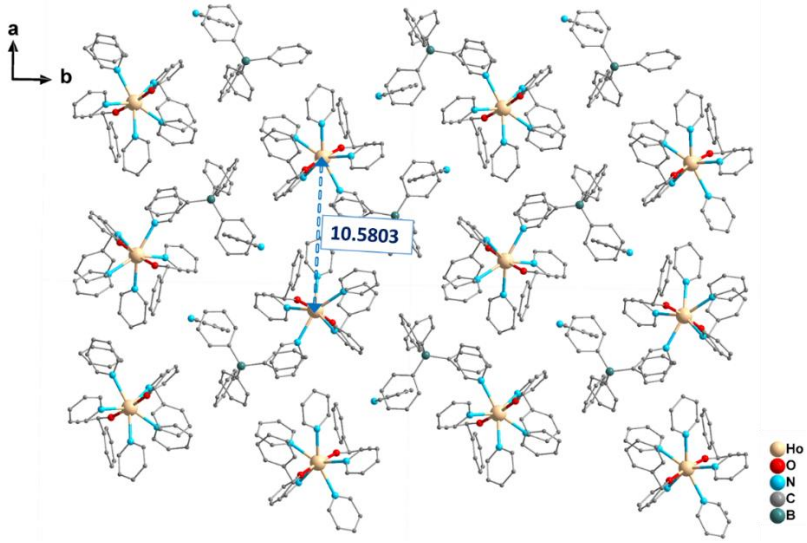

Fig. S7. Packing of **2** in the crystal structure viewed along the *c* axis. H atoms are omitted for clarity.

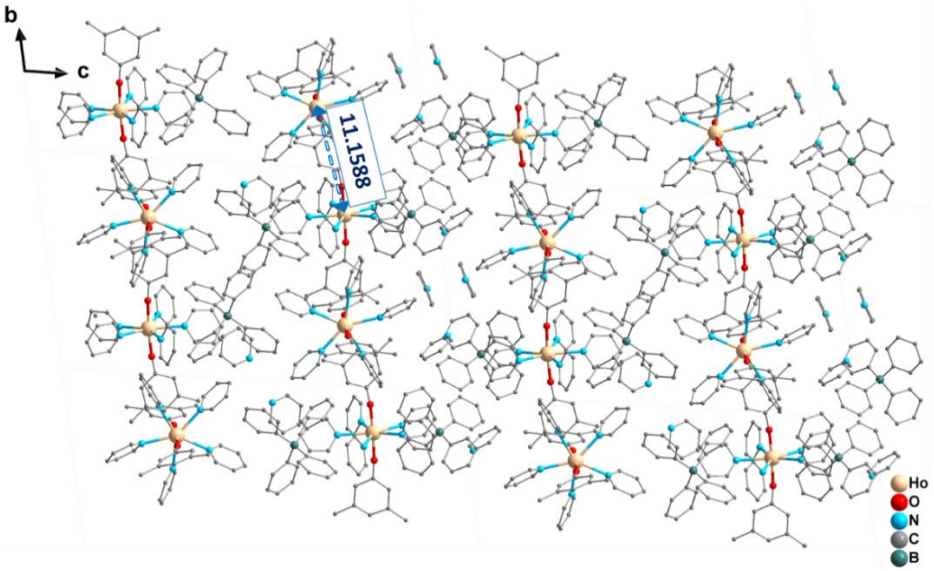

Fig. S8. Packing of **3** in the crystal structure viewed along the *a* axis. H atoms are omitted for clarity.

Magnetic Characterization

Magnetic susceptibility measurements were carried out with a Quantum Design MPMS-XL7 SQUID and MPMS-SQUIDVSM-094 magnetometer. Alternative current susceptibility measurement with frequencies ranging from 1 Hz to 1217 Hz was performed on Quantum Design MPMS-XL7 SQUID magnetometer and ranging from 100 Hz to 10000 Hz was performed on Quantum Design PPMS-14LH on polycrystalline sample. Freshly prepared crystalline samples were embedded in eicosane to avoid any field induced crystal reorientation. Diamagnetic corrections have been applied for the eicosane and for the molecule, the latter being calculated from the Pascal constants.

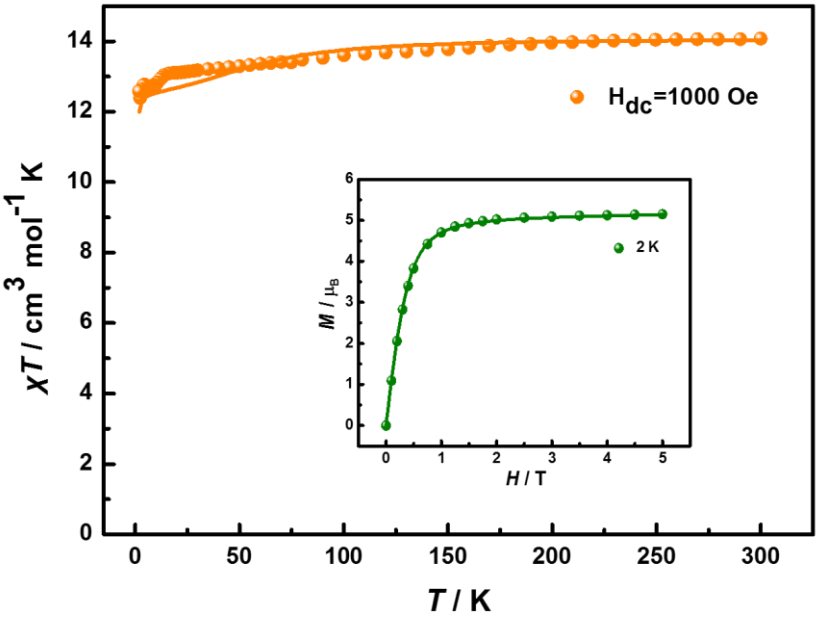

Fig. S9. Temperature dependence of the molar magnetic susceptibility χT products for **1** under a 0.1 T DC field. Inset: magnetization(M) versus H / T for **1**.

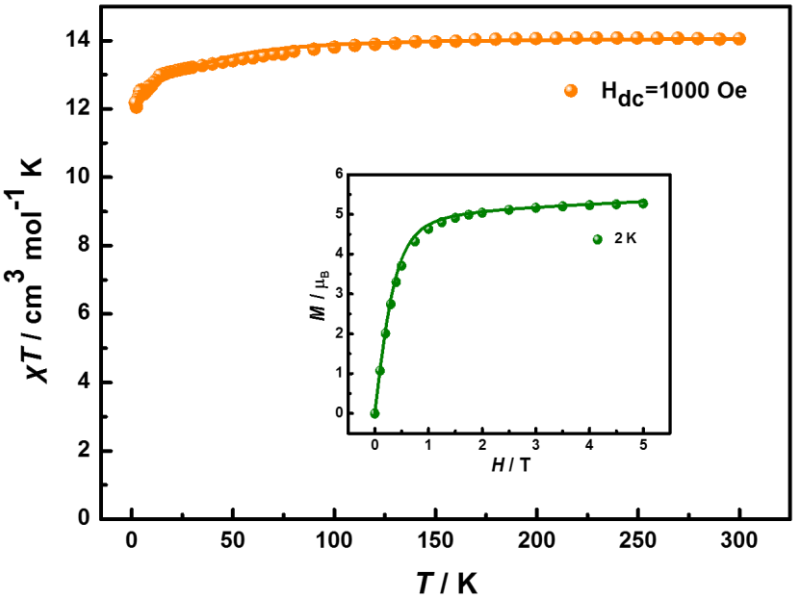

Fig. S10. Temperature dependence of the molar magnetic susceptibility χT products for **2** under a 0.1 T DC field. Inset: magnetization(M) versus H / T for **2**.

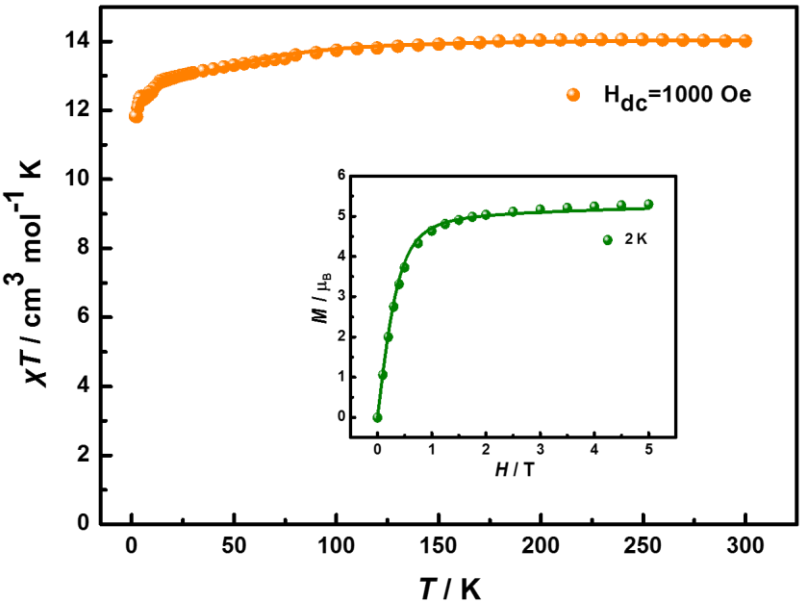

Fig. S11. Temperature dependence of the molar magnetic susceptibility χT products for **3** under a 0.1 T DC field. Inset: magnetization(M) versus H / T for **3**.

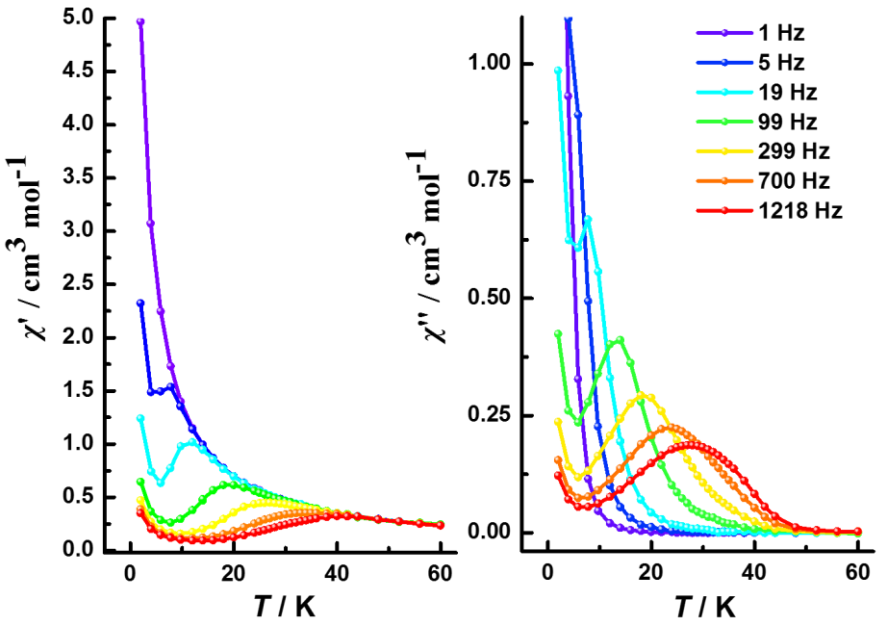

Fig. S12. Temperature dependence of the in-phase (left) and out-of-phase (right) for **1** in a zero DC field with an AC frequency of 1–1218 Hz.

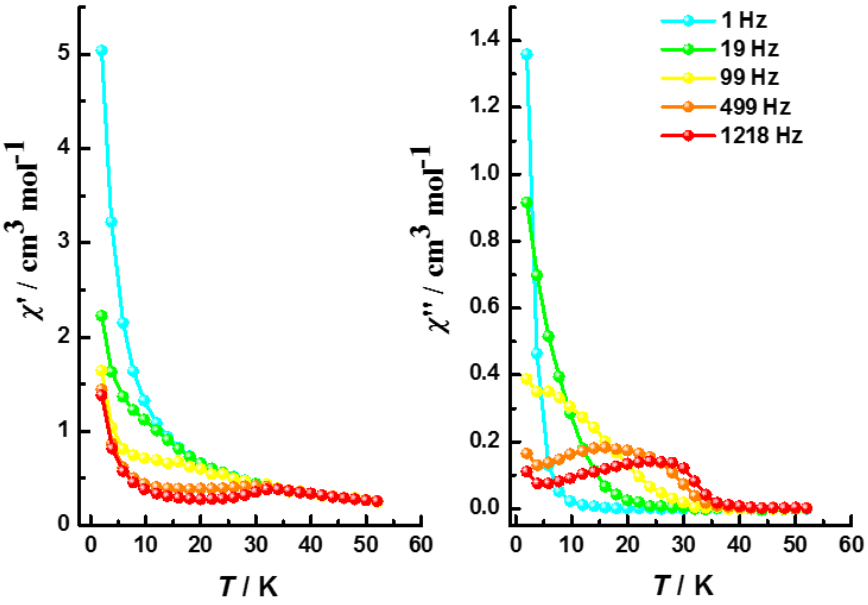

Fig. S13. Temperature dependence of the in-phase (left) and out-of-phase (right) for **2** in a zero DC field with the AC frequency of 1–1218 Hz.

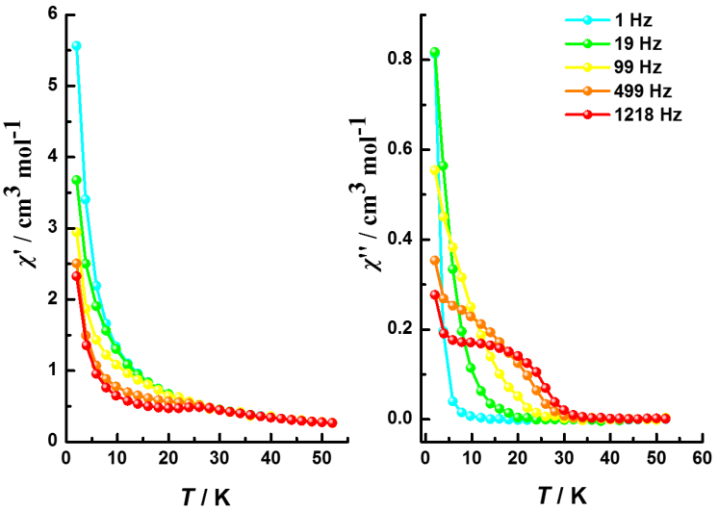

Fig. S14. Temperature dependence of the in-phase (left) and out-of-phase (right) for **3** in a zero DC field with the AC frequency of 1–1218 Hz.

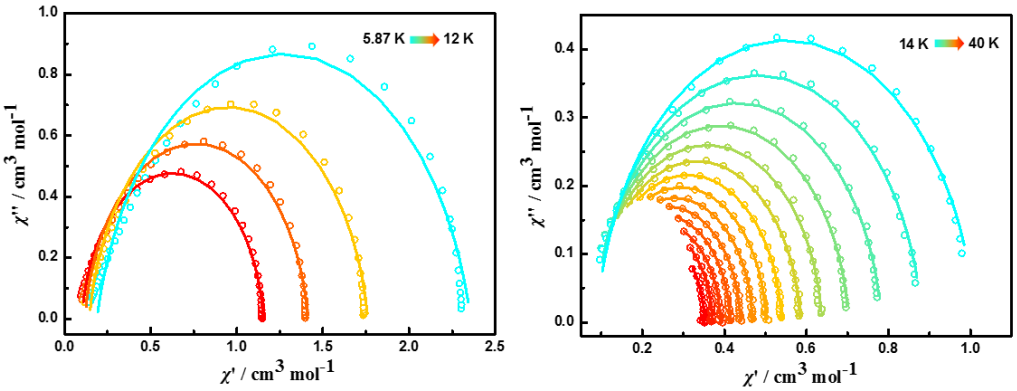

Fig. S15. Cole-Cole plot for the AC susceptibilities in a zero DC field for **1** from 5.87–40 K.

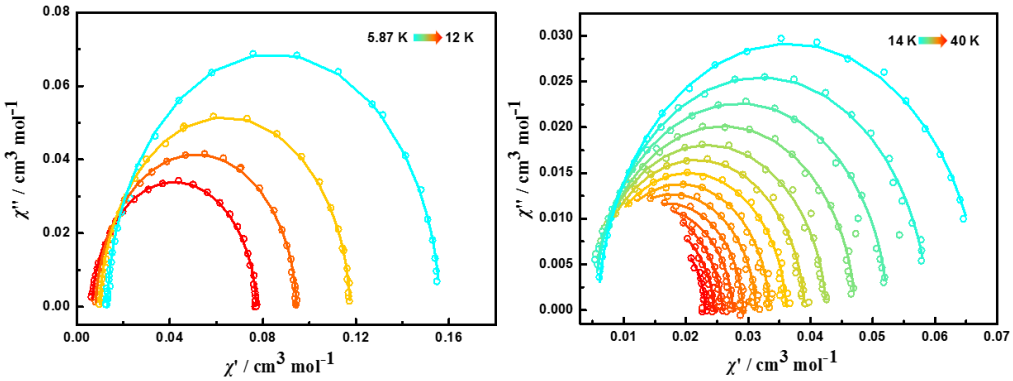

Fig. S16. Cole-Cole plot for the AC susceptibilities in a zero DC field for **1@1Y** from 5.87–40 K.

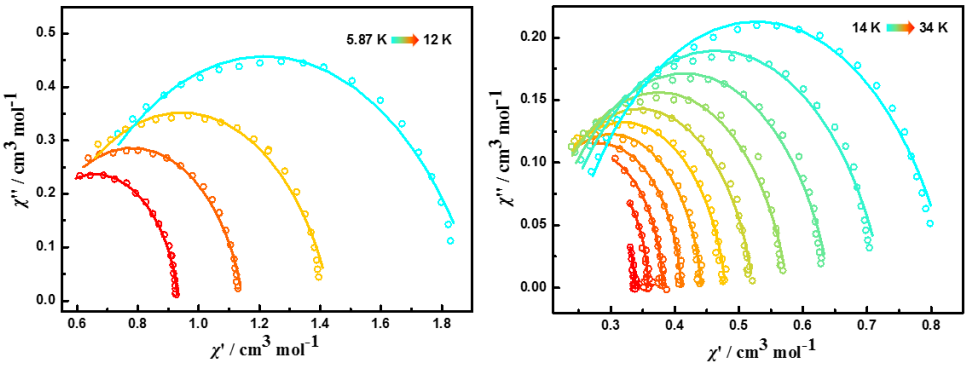

Fig. S17. Cole-Cole plot for the AC susceptibilities in a zero DC field for **2** from 5.87–34 K.

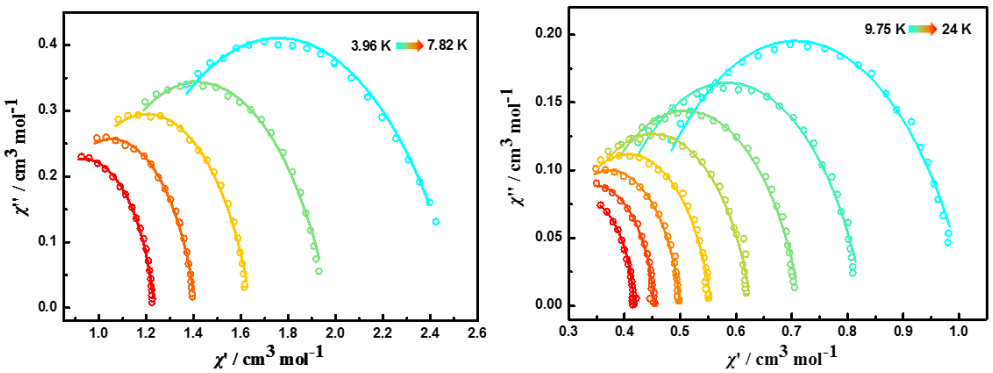

Fig. S18. Cole-Cole plot for the AC susceptibilities in a zero DC field for **3** from 3.96–24 K.

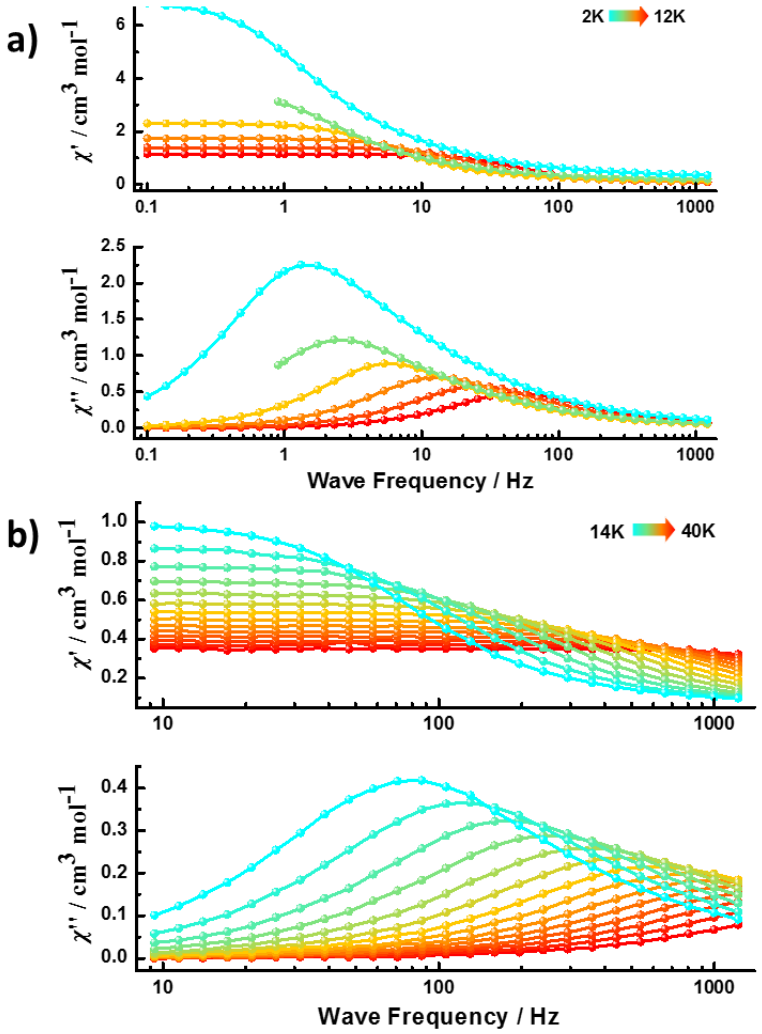

Fig. S19. a) Frequency dependence of the in-phase (χ') and out-of-phase (χ'') magnetic susceptibility in a zero DC field at frequencies ranging from 0.1–1217 Hz and at 2–12 K for **1**. b) Frequency dependence of the in-phase (χ') and out-of-phase (χ'') magnetic susceptibility in a zero DC field at frequencies ranging from 9–1217 Hz and at 14–40 K for **1**.

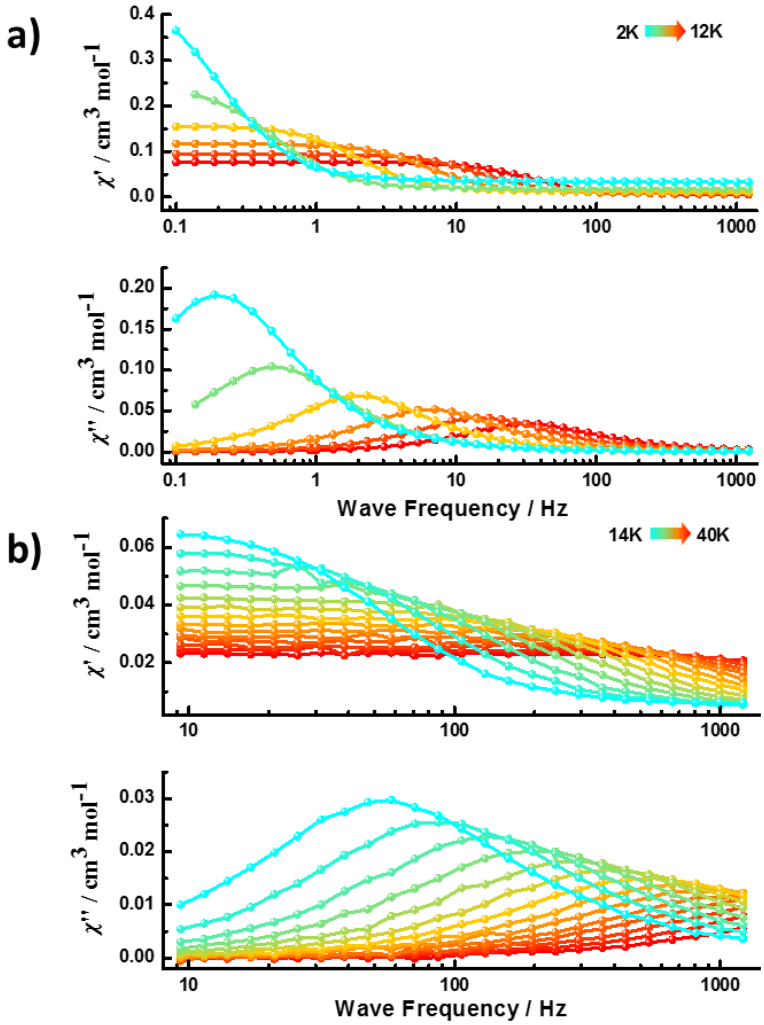

Fig. S20. a) Frequency dependence of the in-phase (χ') and out-of-phase (χ'') magnetic susceptibility in a zero DC field at frequencies ranging from 0.1–1217 Hz and at 2–12 K for **1@1Y**. b) Frequency dependence of the in-phase (χ') and out-of-phase (χ'') magnetic susceptibility in a zero DC field at frequencies ranging from 9–1217 Hz and at 14–40 K for **1@1Y**.

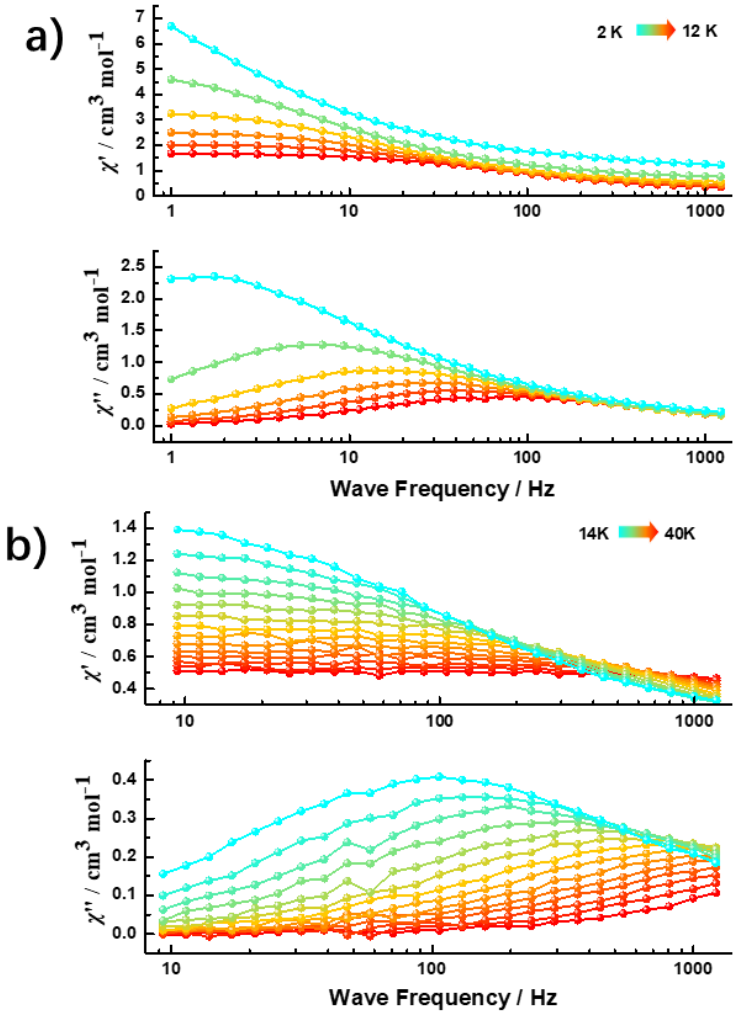

Fig. S21. a) Frequency dependence of the in-phase (χ') and out-of-phase (χ'') magnetic susceptibility in a zero DC field at frequencies ranging from 1–1217 Hz and at 2–12 K for **1-solution**. b) Frequency dependence of the in-phase (χ') and out-of-phase (χ'') magnetic susceptibility in a zero DC field at frequencies ranging from 9–1217 Hz and at 14–40 K for **1-solution**.

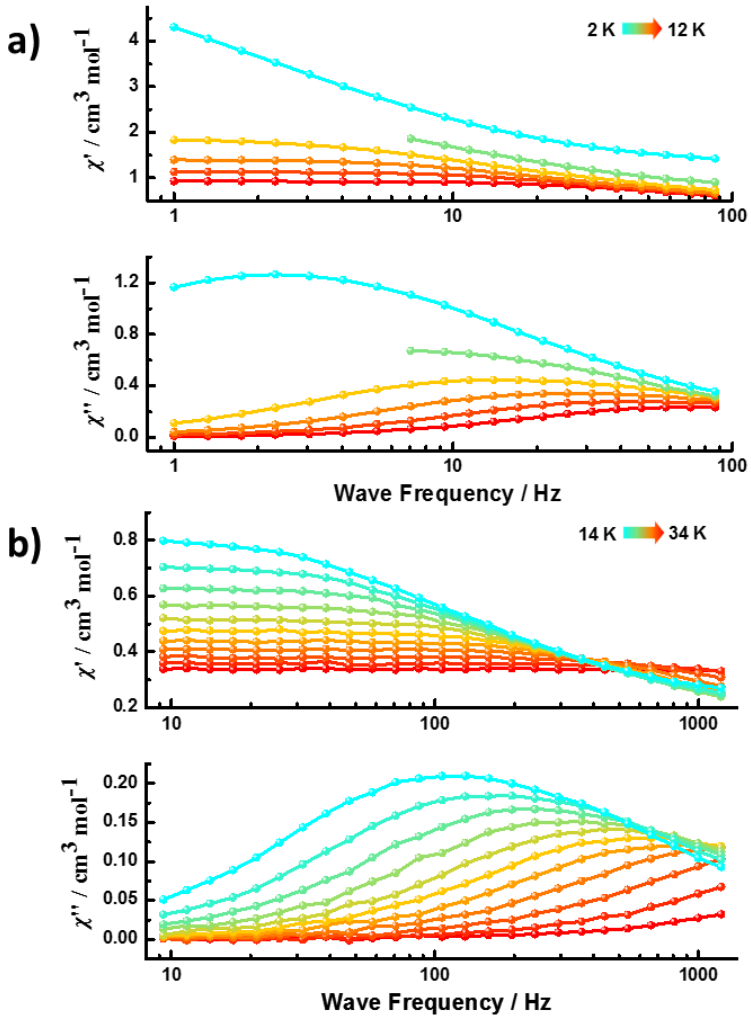

Fig. S22. a) Frequency dependence of the in-phase (χ') and out-of-phase (χ'') magnetic susceptibility in a zero DC field at frequencies ranging from 1–87 Hz and at 2–12 K for **2**. b) Frequency dependence of the in-phase (χ') and out-of-phase (χ'') magnetic susceptibility in a zero DC field at frequencies ranging from 9–1217 Hz and at 14–34 K for **2**.

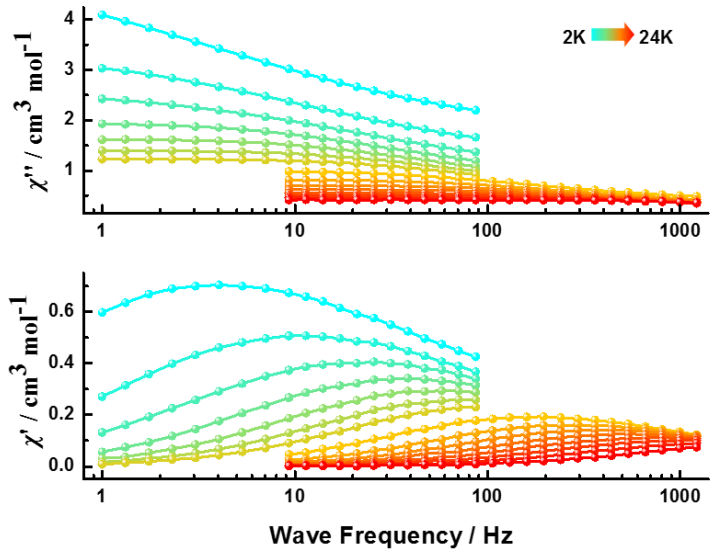

Fig. S23. Frequency dependence of the in-phase (χ') and out-of-phase (χ'') magnetic susceptibility in a zero DC field at 2–24 K for **3**.

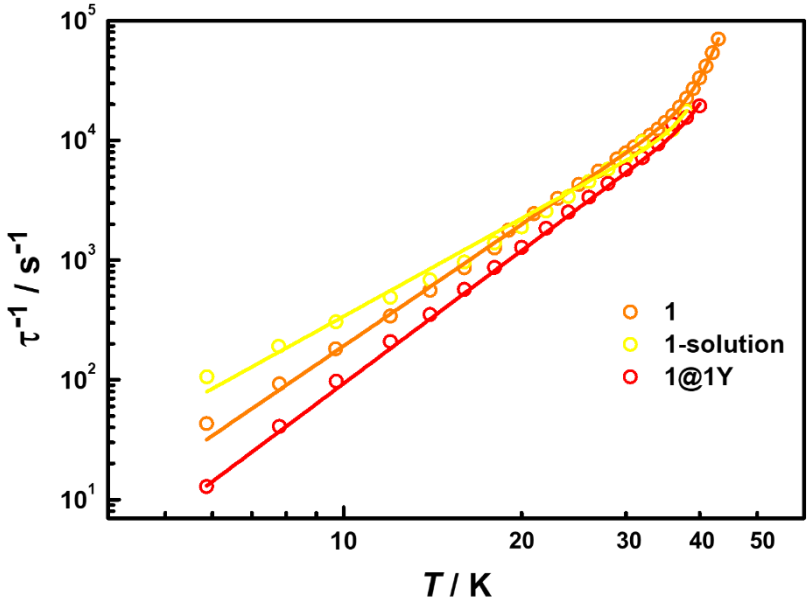

Fig. S24. Arrhenius plot of magnetic relaxation times of **1**, **1@1Y** and **1-Solution**.

The ac fitting parameters for **1@1Y** and **1-Solution**.

	τ_0/s	U_{eff}/K	C/K^{-n} S^{-1}	n
1@1Y	4×10^{-12}(fixed)	711(5)	0.019(1)	3.69(3)
1-Solution	1×10^{-11}(fixed)	640(fixed)	0.6(2)	2.7(1)

* Equation $\tau^{-1} = {\tau_0}^{-1} e^{-U_{eff}/k_B T} + CT^n$ was used for **1@Y** and **1-Solution**.

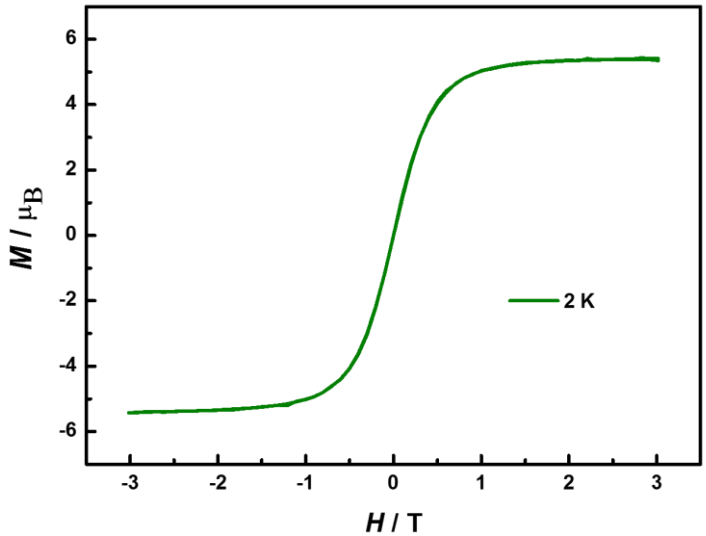

Fig. S25. Magnetic hysteresis measurement of **1** at 2 K at a sweep rate of 14 Oe/s.

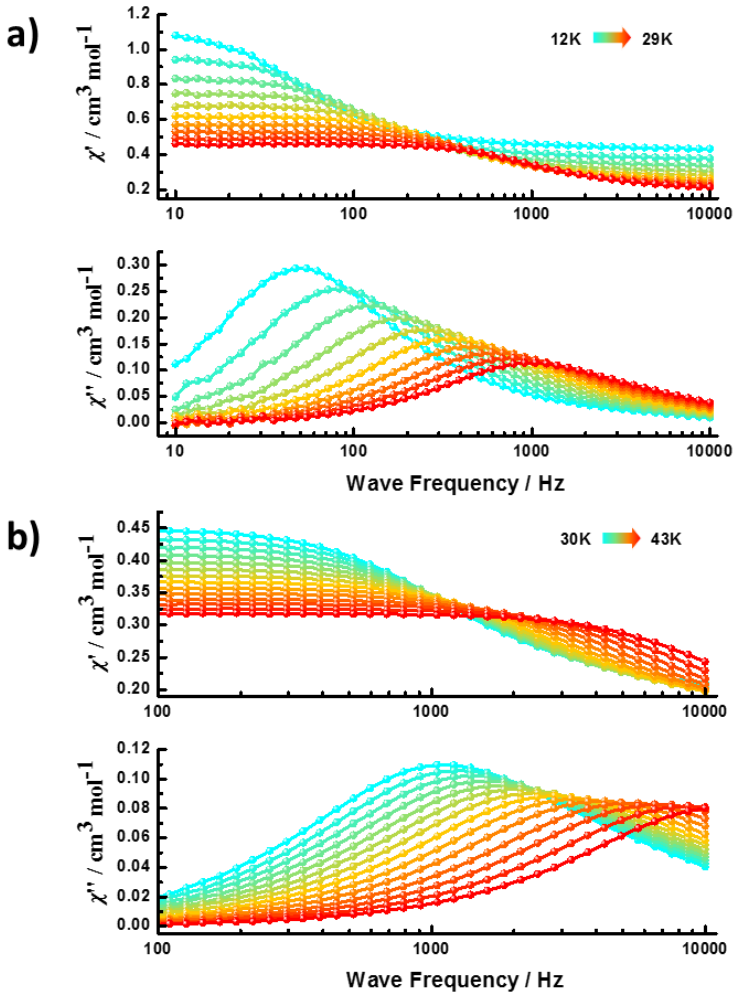

Fig. S26. a) Frequency dependence of the in-phase (χ') and out-of-phase (χ'') magnetic susceptibility in a zero DC field at frequencies ranging from 100–10000 Hz and at 12–29 K for **1**. b) Frequency dependence of the in-phase (χ') and out-of-phase (χ'') magnetic susceptibility in a zero DC field at frequencies ranging from 100–10000 Hz and at 30–43 K for **1**.

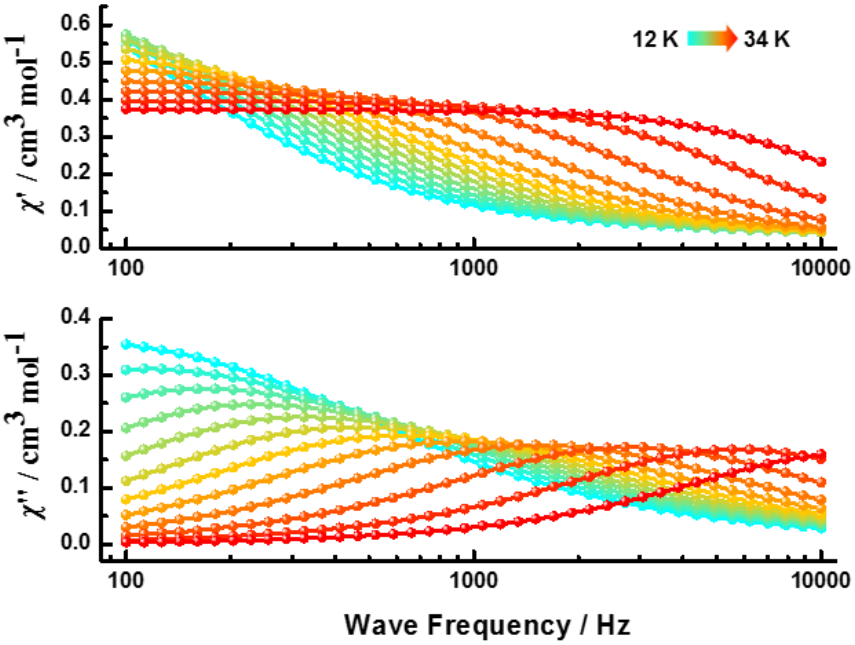

Fig. S27. Frequency dependence of the in-phase (χ') and out-of-phase (χ'') magnetic susceptibility in a zero DC field at frequencies ranging from 100–10000 Hz and at 12–34 K for **2**.

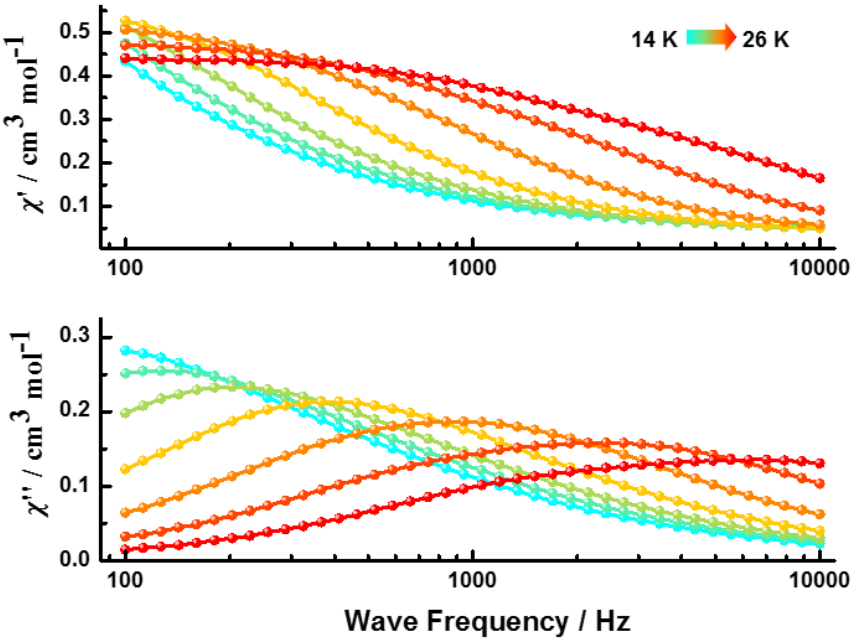

Fig. S28. Frequency dependence of the in-phase (χ') and out-of-phase (χ'') magnetic susceptibility in a zero DC field at 14–26 K for **3**.

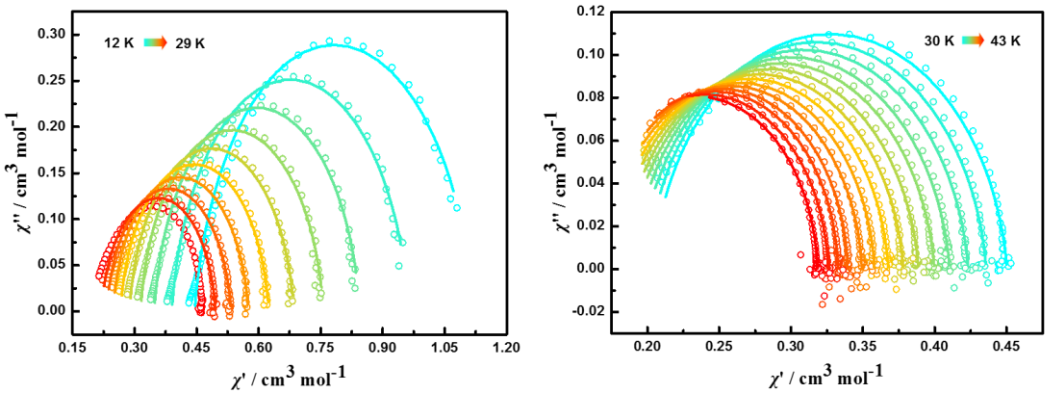

Fig. S29. Cole-Cole plot for the AC susceptibilities in a zero DC field for **1** at frequencies ranging from 100–10000 Hz and 12–43 K.

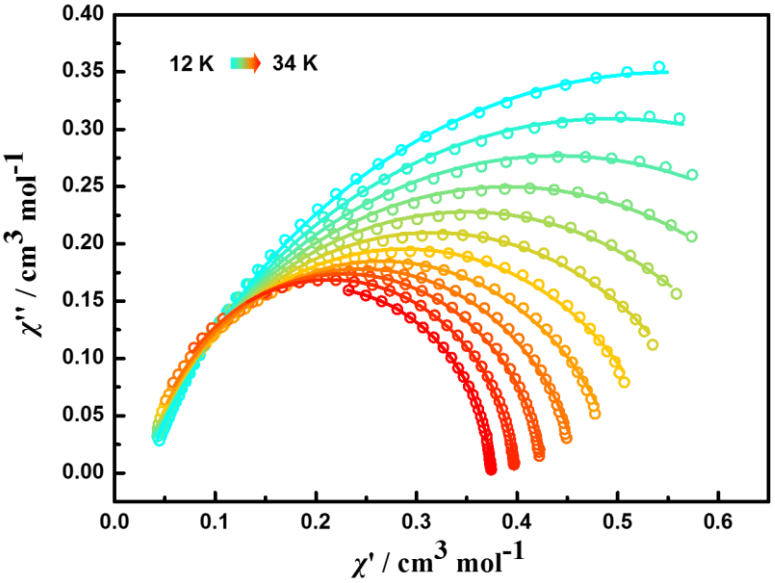

Fig. S30. Cole-Cole plot for the AC susceptibilities in a zero DC field for **2** at frequencies ranging from 100–10000 Hz and 12–34 K.

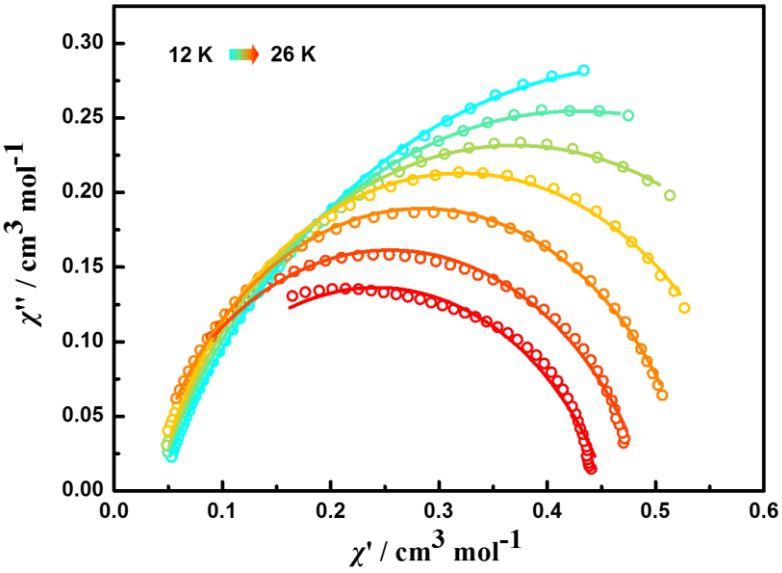

Fig. S31. Cole-Cole plot for the AC susceptibilities in a zero DC field for **3** at frequencies ranging from 100–10000 Hz and 12–26 K.

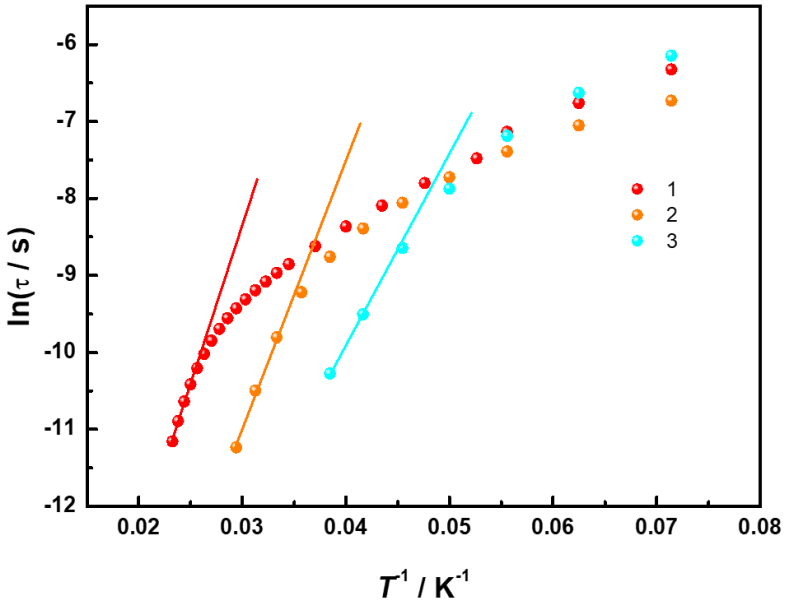

Fig. S32. Arrhenius plot of magnetic relaxation times of **1** (red), **2** (orange) and **3** (cyan). The solid lines represent data fitting with Arrhenius law ($\tau^{-1} = {\tau'_0}^{-1} e^{-U'_{eff}/kT}$).

Table S5. The fitting parameters solely using Arrhenius law in high temperatures for **1**–**3**.

	τ'_0 / s	U'_{eff} / K *	R^2
1	1.42(3)×10^{-9}	427(7)	0.9973
2	3.21(4)×10^{-9}	363(2)	0.9937
3	2.22(7)×10^{-8}	232(2)	0.9993

* The U'_{eff} shown here by solely fitting of the relaxation times in high temperatures **cannot** be truly equal to the effective energy barrier (U_{eff}), because in all three cases those points we observed are dominated by both Raman and Orbach processes, not solely by Orbach process. Thus, we would rather consider the U_{eff} fitted with Raman + Orbach (in the main text) as the energy barrier for magnetization reversal.

Here, we take **1** for example to discuss the gap between this U'_{eff} = 427(7) with U_{eff} = 715(6) K in the main text:

We refer to the below fitting method as **Method 2**, and the simultaneous fitting with Raman + Orbach (in the main text) as **Method 1**.

Method 2:

Firstly, we plot the τ^{-1} vs. T curve in log–log scale as shown in Fig. S33. The dots between 12 and 36 K show a good linearity which can be fitted by Raman process, giving C = 0.043(3) $S^{-1}K^{-n}$, n = 3.56(2). We can observe an obvious deviation from Raman process at higher temperatures.

Secondly, we extrapolate the contribution of τ^{-1}_{Raman} from the parameters obtained above in the temperature range of 37–43 K. Subtracting τ^{-1}_{Raman} from the total τ^{-1}, we can get (τ^{-1}_{origin}–τ^{-1}_{Raman}) in this temperature range.

Thirdly, we plot the (τ^{-1}_{origin}–τ^{-1}_{Raman}) vs. T curve (Fig. S34), and get a linear relationship from 37 to 43 K. The best fit by Arrhenius equation, $\tau^{-1} = {\tau_0}^{-1} e^{-U_{eff}/k_B T}$, gives τ_0 = 7.8(8)×10^{-13} s and U_{eff} = 741(5) K.

At last, we extrapolate all the τ^{-1}_{Raman} and τ^{-1}_{Orbach} in the temperature range of 12–43 K from the parameters obtained above, and list the τ^{-1}_{total}, and (τ^{-1}_{origin}–τ^{-1}_{Raman}) together in Table S6.

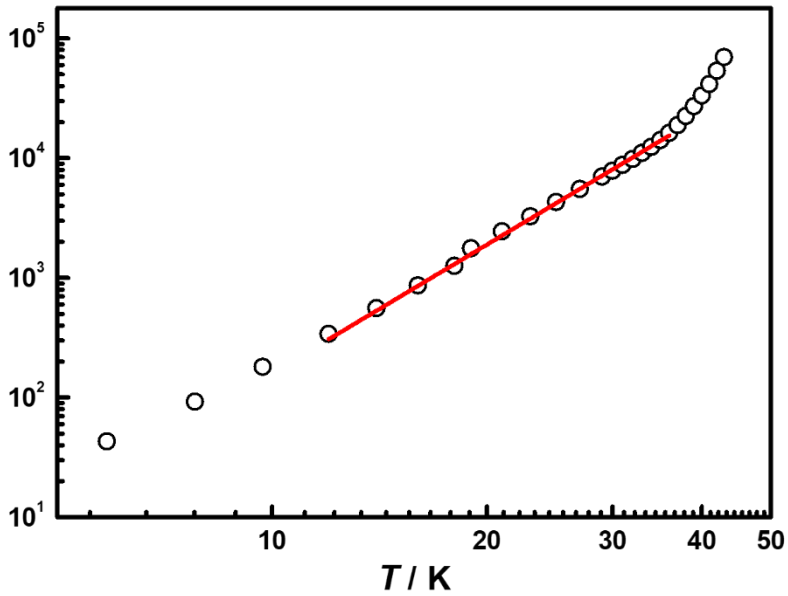

Fig. S33. Temperature dependence of the relaxation times for **1**. Red line is the fit to the equation $\tau^{-1} = CT^n$, where C = 0.043(3) $S^{-1}K^{-n}$, n = 3.56(2).

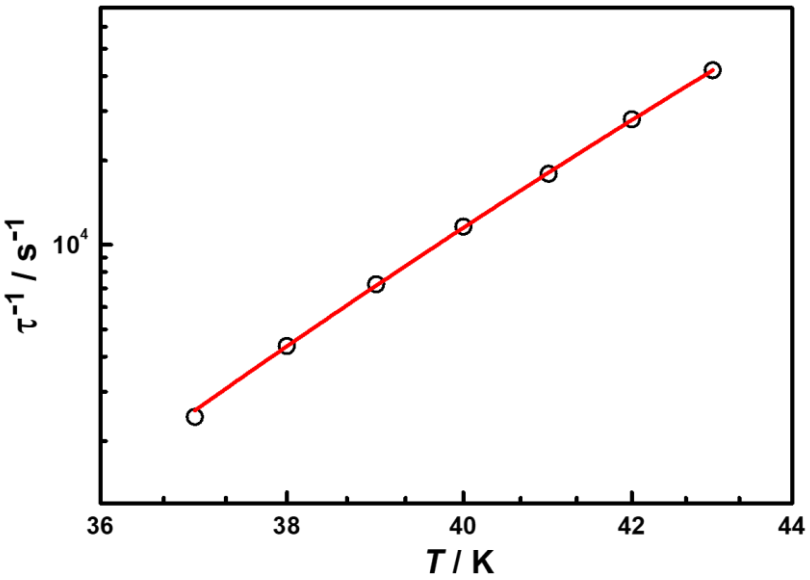

Fig. S34. Temperature dependence of the relaxation times (the contribution of Raman process is removed, see above) for **1** between 37 and 43 K. Red line is the fit to the equation $\tau^{-1} = {\tau_0}^{-1} e^{-U_{eff}/k_B T}$, giving τ_0= 7.8(8)×10^{-13} s, U_{eff}= 741(5) K.

Table S6. Relaxation times corresponding to different relaxation processes of compound **1** by **Method 2**.

T / K	τ^{-1}_{origin} / s^{-1} (experimental value)	τ^{-1}_{Raman}# / s^{-1} (fitted value)	(τ^{-1}_{origin}–τ^{-1}_{Raman}) / s^{-1}	τ^{-1}_{Orbach}# / s^{-1} (fitted value)
5.86	43.14299	23.29078	19.85222	1.5569E-43
7.78	92.65658	63.87866	28.77792	5.55884E-30
9.7	180.78166	140.0799	40.70176	8.56061E-22
12	339.95389	298.78149	41.1724	1.95586E-15
14	558.91086	517.23066	41.6802	1.32567E-11
16	863.53117	832.0235	31.50767	9.9028E-9
18	1257.96423	1265.4313	-7.46708	1.70046E-6
19	1772.38256	1534.02089	238.36167	1.48435E-5
21	2443.48359	2190.63057	252.85301	6.09018E-4
23	3274.23653	3028.44403	245.7925	0.0131
25	4293.12421	4075.06825	218.05596	0.1724
27	5537.28728	5359.48989	177.79739	1.549
29	7000.80205	6912.02544	88.77661	10.28131
30	7836.67566	7798.66244	38.01322	24.09615
31	8791.58242	8764.27681	27.30562	53.45426
32	9833.69468	9813.0131	20.68158	112.82096
33	11071.61605	10949.09141	122.52464	227.58111
34	12415.48794	12176.80637	238.68157	440.51061
35	14110.57789	13500.52612	610.05177	821.08251
36	16203.29669	14924.69134	1278.60535	1478.40464
37	18887.01636	16453.81437	2433.20199	2578.65995
38	22451.66376	18092.47826	4359.1855	4367.96354
39	27080.52192	19845.33601	7235.1859	7201.5544
40	33328.89442	21717.10968	11611.78474	11580.20172
41	41618.08136	23712.58963	17905.49173	18194.62389
42	53887.2942	25836.63378	28050.66042	27978.59487
43	70042.67653	28094.16686	41948.50968	42171.25181

τ^{-1}_{Raman} was extrapolated from the parameters obtained by fitting the data in Fig. S33.
τ^{-1}_{Orbach} was extrapolated from the parameters obtained by fitting the data in Fig. S34.

In comparison, we also list the τ^{-1}_{Raman}, (τ^{-1}_{origin}–τ^{-1}_{Raman}), and τ^{-1}_{Orbach} extrapolated from the parameters in the main text (**Method 1**) in Table S7. When we look at Table S6 and Table S7 closely, no matter which method we take, the τ^{-1}_{Raman} is absolutely dominated in τ^{-1}_{origin} in the power-law dependence region (12–36 K), and the contribution of τ^{-1}_{Orbach} is significant lower than that of τ^{-1}_{Raman} (almost less than 1/10). That is why we can obtain reliable Raman parameters and extrapolate them to the Orbach region. However, it can be seen that the contributions of τ^{-1}_{Orbach} and τ^{-1}_{Raman} are almost at the same level, and τ^{-1}_{Raman} cannot be neglected at all in the Orbach region (37–43 K). If we substrate this important Raman contribution from τ^{-1}_{origin}, and then fit these data with only Arrhenius law, similar energy barrier can be achieved around 740 K. The fitting results by both Methods listed in Table S8 are very similar. The small difference between the parameters comes from the neglect of the low-temperature Orbach process. In general, fitting with **Method 1** is more in line with the real situation.

Table S7. Relaxation times corresponding to different relaxation processes of compound **1** by **Method 1**.

T / K	τ^{-1}_{origin} / s^{-1} (experimental value)	τ^{-1}_{total} * / s^{-1} (fitted value)	τ^{-1}_{Raman} * / s^{-1} (fitted value)	(τ^{-1}_{origin}–τ^{-1}_{Raman}) / s^{-1}	τ^{-1}_{Orbach} * / s^{-1} (fitted value)
5.86	43.14299	40.73184	30.73184	12.41115	6.6388E-42
7.78	92.65658	90.09504	80.09504	12.56154	8.27117E-29
9.7	180.78166	178.80413	168.80413	11.97753	6.74304E-21
12	339.95389	356.51913	346.51913	-6.56524	9.40054E-15
14	558.91086	593.455	583.455	-24.54413	4.73147E-11
16	863.53117	926.26299	916.26299	-52.73181	2.82734E-8
18	1257.96423	1374.3182	1364.31819	-106.35397	4.0812E-6
19	1772.38256	1647.87888	1637.87885	134.50371	3.3114E-5
21	2443.48359	2307.18539	2297.18419	146.2994	0.0012
23	3274.23653	3134.19346	3124.17022	150.06631	0.02324
25	4293.12421	4151.53411	4141.25365	151.87055	0.28045
27	5537.28728	5383.94567	5371.60569	165.68159	2.33997
29	7000.80205	6863.68443	6839.11388	161.68817	14.57054
30	7836.67566	7712.63537	7669.45394	167.22172	33.18143
31	8791.58242	8650.00505	8568.34861	223.23381	71.65643
32	9833.69468	9696.4458	9538.97102	294.72366	147.47478
33	11071.61605	10885.05781	10584.53344	487.08261	290.52437
34	12415.48794	12268.23998	11708.28653	707.20141	549.95344
35	14110.57789	13927.28469	12913.51861	1197.05928	1003.76609
36	16203.29669	15985.38506	14203.55493	1999.74176	1771.83013
37	18887.01636	18624.75192	15581.7571	3305.25926	3032.99482
38	22451.66376	22108.53551	17051.52238	5400.14138	5047.01313
39	27080.52192	26808.20858	18616.28309	8464.23883	8181.9255
40	33328.89442	33236.99512	20279.50608	13049.38833	12947.48904
41	41618.08136	42089.82226	22044.69215	19573.38921	20035.13011
42	53887.2942	54290.13852	23915.3755	29971.9187	30364.76302
43	70042.67653	71043.78309	25895.12326	44147.55327	45138.65983

* τ^{-1}_{total} was obtained by fitting the data with Raman + Orbach processes (**Method 1**).
* τ^{-1}_{Raman} was extrapolated from the parameters of Raman term in **Method 1**.
* τ^{-1}_{Orbach} was extrapolated from the parameters of Orbach term in **Method 1**.

Table S8. The magnetic parameters of compound **1** fitted by **Method 1** and **Method 2**.

Methods	τ_0/s	U_{eff}/K	C/K^{-n} S^{-1}	n
Method 2: Single Raman (Fig. S33)	-	-	0.043(3)	3.56(2)
Method 2: Single Orbach (Fig. S34)	$7.8(8)\times10^{-13}$	741(5)	-	-
Method 1: Total (Fig. 2)	$1.3(2)\times10^{-12}$	715(6)	0.080(9)	3.38(3)

Electronic Structure Calculations.

Ab initio calculations at SA-CASSCF/RASSI level were performed on program MOLCAS 8.0[1] and the structure was originally taken from the X-Ray structure of **1** - **3**. The basis sets were chosen from the ANO-RCC library[2] as have been used in many works[3, 4]. The Ho atom was treated with VTZP quality, then the related N and O atoms with VDZP quality and others (Si, C and H atoms) with VDZ quality. The active space of the CASSCF method included 10 electrons in 7 4f orbitals of Ho(III) ion. The state-averaged CASSCF orbitals of the quintets, triplets and singlets were optimized with 35, 210 and 196 states, respectively, with the RASSCF module. 35, 117 and 75 quintets, triplets and singlets were chosen to constructe and diagonalise in spin-orbit (SO) coupling Hamiltonian with the RASSI module. These computed SO states were written into the SINGLE_ANISO program[5] to compute the *g*-tensors, crystal field parameters, magnetic energy levels as well as local magnetic susceptibility and magnetization for the doublets of the ground J = 8 multiplet of the ^{5}I term for Ho(III). The two electron integrals were Cholesky decomposed with a threshold of 1×10^{-8} to account for the accuracy.

Table S9. SA-CASSCF/RASSI calculated electronic states for **1**.

Levels	Energy (cm^{-1})	g_z	g_z Angle (°)	Δ_{tun} (cm^{-1})	Wavefunction [a]
1	0	19.87	--	0.0005	50.0%|+8> + 50.0%|−8>
2	5×10^{-4}				50.0%|−8> + 50.0%|+8>
3	348.62	17.25	0.5	0.03	49.4%|+7> + 49.4%|−7>
4	348.65				49.4%|−7> + 49.4%|+7>
5	477.23	12.57	13.5	0.66	39.0%|+6> + 39.0%|−6>
6	477.89				40.6%|−6> + 40.6%|+6>
7	487.34	12.58	71.3	5.43	20.0%|+3> + 26.2%|0> + 20.0%|−3>
8	492.77				25.1%|+4> + 11.0%|+1> + 11.0%|−1> + 25.1%|−4>
9	495.86	10.99	50.2	2.76	13.2%|+3> + 23.0%|+2> + 23.0%|−2> + 13.2%|−3>
10	498.62				15.9%|+5> + 17.0%|+2> + 17.0%|−2> + 15.9%|−5>
11	505.68	9.21	70.0	3.42	15.6%|+5> + 16.1%|+4> + 10%|+1> + 10%|0> + 10%|−1> + 16.1%|−4> + 15.6%|−5>
12	509.10				25.2%|−3> + 25.2%|+3>
13	516.16	8.98	80.3	7.48	13.7%|+5> + 16.4%|+4> + 16.4%|−4> + 13.7%|−5>
14	523.64				12.1%|+3> + 13.0%|+2> + 17.7%|+1> + 17.7%|−1> + 13.0%|−2> + 12.1%|−3>
15	527.39	6.30	71.9	7.92	16.1%|+5> + 23.2%|+2> + 23.2%|−2> + 16.1%|−5>
16	535.31				14.0%|+4> + 16.2%|+1> + 20.5%|0> + 16.2%|−1> + 14.0%|−4>
17	536.69	--	--	--	11.3%|+1> + 30.5%|0> + 11.3%|−1>

[a] Only components with > 10% contribution are given, rounded to the nearest percent.

Table S10 *Ab initio* calculated crystal field parameters for **1**.

Crystal Field Parameter	Value / cm^{-1}
B_2^{-2}	-0.12607134332469E-01
B_2^{-1}	-0.15613994394705E+00
B_2^0	-0.21308117562185E+01
B_2^1	0.26967147170861E-01
B_2^2	0.19501726645468E-01
B_4^{-4}	-0.12544061609360E-03
B_4^{-3}	-0.77133988917601E-03
B_4^{-2}	0.45344395041267E-03
B_4^{-1}	-0.40833095833459E-02
B_4^0	-0.65478290243827E-02
B_4^1	0.15008485541886E-02
B_4^2	0.15463519344286E-03
B_4^3	-0.58251227457992E-02
B_4^4	0.28648743604824E-03
B_6^{-6}	-0.18779200035480E-04
B_6^{-5}	0.22968837446684E-03
B_6^{-4}	0.11064184808425E-04
B_6^{-3}	0.14805646048709E-04
B_6^{-2}	-0.57112979752424E-06
B_6^{-1}	-0.66186303307803E-06
B_6^0	-0.20319974949878E-04
B_6^1	-0.23636552508808E-05
B_6^2	-0.41962986837867E-05
B_6^3	0.11293087536292E-03
B_6^4	-0.23390694355601E-04
B_6^5	0.13131497926902E-04
B_6^6	0.16186681457306E-04

Table S11. SA-CASSCF/RASSI calculated electronic states for **2**.

Levels	Energy (cm^{-1})	g_z	g_z Angle (°)	Δ_{tun} (cm^{-1})	Wavefunction [a]
1	0	19.87	--	0.002	48.9%|+8> + 48.9%|−8>
2	0.002				48.9%|−8> + 48.9%|+8>
3	247.55	17.40	7.6	0.03	42.8%|+7> + 42.8%|−7>
4	247.58				42.8%|−7> + 42.8%|+7>
5	387.25	12.86	18	5.84	22.4%|+6> + 10%|+5> + 10%|+1> + 10%|−1> + 10%|−5> + 22.4%|−6>
6	393.09				29.3%|+6> + 12%|+5> + 12%|−5> + 29.3%|−6>
7	402.52	12.89	78	8.93	16%|+2> + 15%|+1> + 15%|−1> + 16%|−2>
8	411.45				28%|−2> + 28%|+2>
9	418.46	10.02	82	18.58	13%|+1> + 42%|0> + 13%|−1>
10	437.04				10%|+3> + 27%|+1> + 27%|−1> + 10%|−3>
11	446.75	12.38	87	19.94	26%|+3> + 25%|0> + 26%|−3>
12	466.69				24%|+4> + 14%|+2> + 14%|−2> + 24%|−4>
13	473.00	10.81	7.2	1.38	12%|+6> + 24%|+5> + 10%|+4> + 10%|−4> + 24%|−5> + 12%|−6>
14	474.38				16%|+5> + 19%|+4> + 19%|−4> + 16%|−5>
15	489.49	8.55	84	10.24	14%|+5> + 19%|+4> + 10%|+1> + 10%|−1> + 19%|−4> + 14%|−5>
16	499.73				27%|+3> + 13%|+2> + 13%|−2> + 27%|−3>
17	501.17	--	--	--	14%|+3> + 14%|+2> + 14%|−2> + 14%|−3>

[a] Only components with > 10% contribution are given, rounded to the nearest percent.

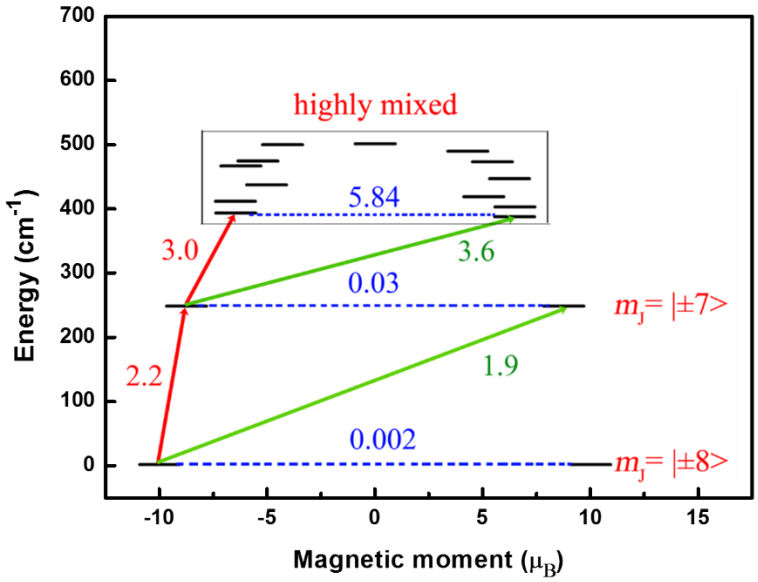

Fig. S35. Energy levels of pseudo doublets for **2** along with their wavefunction compositions. The horizontal blue dashed lines show the tunnelling transitions within each doublets and the numbers are tunnelling gaps (Δ_{tun}) in Tables S8. The non-horizontal solid lines show the spin-phonon transition paths and the numbers stand for averaged transition moments in Tables S17.

Table S12. *Ab initio* calculated crystal field parameters for **2**.

Crystal Field Parameter	Value / cm^{-1}
B_2^{-2}	0.48230944374443E-01
B_2^{-1}	0.62393272052128E-01
B_2^0	-0.19608941579894E+01
B_2^1	0.11469345205263E+01
B_2^2	0.49398193631712E-01
B_4^{-4}	0.33739344011489E-03
B_4^{-3}	0.84029116821722E-03
B_4^{-2}	0.31326890505000E-04
B_4^{-1}	-0.29379167388188E-03
B_4^0	-0.56907871209074E-02
B_4^1	0.14968698896984E-01
B_4^2	-0.15944429224467E-02
B_4^3	-0.13060059614768E-02
B_4^4	0.15687424181448E-02
B_6^{-6}	0.20319655156585E-04
B_6^{-5}	0.56451964759548E-04
B_6^{-4}	-0.90251589317414E-05
B_6^{-3}	0.83664348387183E-05
B_6^{-2}	-0.47403549582393E-06
B_6^{-1}	0.14938112613182E-04
B_6^0	-0.34949042482241E-05
B_6^1	-0.10575423441150E-03
B_6^2	0.63291936589085E-04
B_6^3	-0.41051978736938E-04
B_6^4	-0.23170127406505E-04
B_6^5	0.69711717431715E-04
B_6^6	0.69417131848123E-04

Table S13. SA-CASSCF/RASSI calculated electronic states for **3**.

Levels	Energy (cm^{-1})	g_z	g_z Angle (°)	Δ_{tun} (cm^{-1})	Wavefunction [a]
1	0	19.85	--	0.008	49.6%|+8> + 49.6%|−8>
2	0.008				49.6%|−8> + 49.6%|+8>
3	209.30	17.23	0.6	0.31	48.8%|+7> + 48.8%|−7>
4	209.61				48.9%|−7> + 48.9%|+7>
5	291.90	16.37	89	8.13	64.4%|0>
6	300.03				32%|+1> + 11%|0> + 32%|−1>
7	312.93	14.24	79	15.43	43%|+1> + 43%|−1>
8	328.36				35%|+2> + 12%|0> + 35%|−2>
9	338.40	11.73	1.4	7.42	39%|+6> + 39%|−6>
10	345.82				42%|+6> + 42%|−6>
11	348.44	12.20	89	18.47	34%|+2> + 34%|−2>
12	366.91				41%|+3> + 41%|−3>
13	404.56	0.86	89	2.18	41%|+5> + 41%|−5>
14	406.74				39%|+3> + 39%|−3>
15	408.54	8.63	89	7.72	40%|+5> + 40%|−5>
16	416.26				39%|+4> + 39%|−4>
17	417.10	--	--	--	42%|+4> + 42%|−4>

[a] Only components with > 10% contribution are given, rounded to the nearest percent.

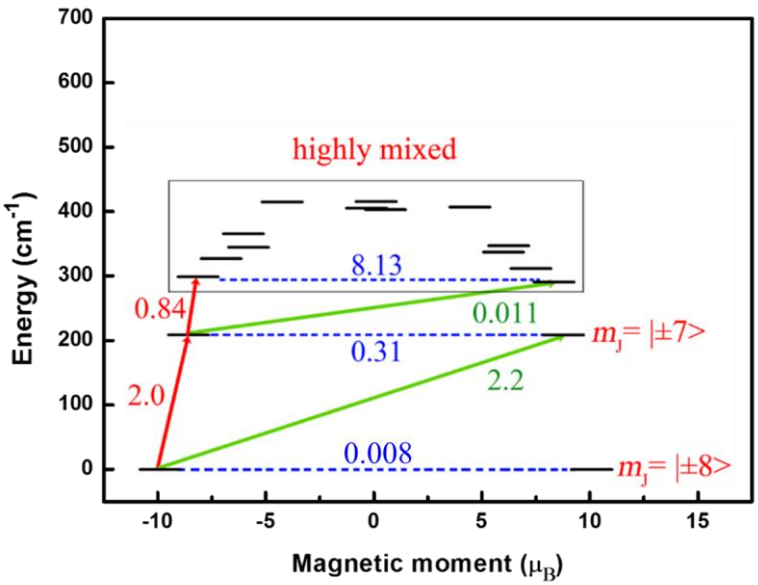

Fig. S36. Energy levels of pseudo doublets for **3** along with their wavefunction compositions. The horizontal blue dashed lines show the tunnelling transitions within each doublets and the numbers are tunnelling gaps (Δ_{tun}) in Tables S10. The non-horizontal solid lines show the spin-phonon transition paths and the numbers stand for averaged transition moments in Tables S18.

Table S14 *Ab initio* calculated crystal field parameters for **3**.

Crystal Field Parameter	Value / cm^{-1}
B_2^{-2}	0.75899946507017E-04
B_2^{-1}	-0.25224772976718E-03
B_2^0	-0.14705268734652E+01
B_2^1	0.22826832259027E+00
B_2^2	0.10935891567312E+00
B_4^{-4}	-0.50790800010268E-05
B_4^{-3}	0.17349602533555E-04
B_4^{-2}	0.93112074584354E-06
B_4^{-1}	-0.36248602098607E-05
B_4^0	-0.58654891377962E-02
B_4^1	0.47428440948608E-02
B_4^2	0.36865010519513E-03
B_4^3	0.11054291437894E-01
B_4^4	-0.24371637912238E-02
B_6^{-6}	-0.28228447588059E-06
B_6^{-5}	-0.46511025922677E-06
B_6^{-4}	0.10216056301828E-06
B_6^{-3}	-0.31220510094880E-06
B_6^{-2}	-0.15561104752872E-07
B_6^{-1}	0.52724675327904E-08
B_6^0	0.45136029091016E-05
B_6^1	-0.46705633020734E-05
B_6^2	-0.28193952107251E-05
B_6^3	-0.20310157092383E-03
B_6^4	0.57204047502745E-04
B_6^5	-0.17961830010250E-03
B_6^6	-0.87564534703182E-04

Table S15. CASSCF computed Mullikan charges.

Atom label	**1**	**2**	**3**
Ho	2.4649	2.4549	2.4650
O1	-1.2678	-1.0662	-0.9858
O2	-1.2675	-1.0680	-0.9858
N1	-0.3665	-0.3653	-0.3795
N2	-0.3731	-0.3617	-0.3690
N3	-0.3641	-0.3511	-0.3690
N4	-0.3717	-0.3600	-0.3728
N5	-0.3716	-0.3606	-0.3728

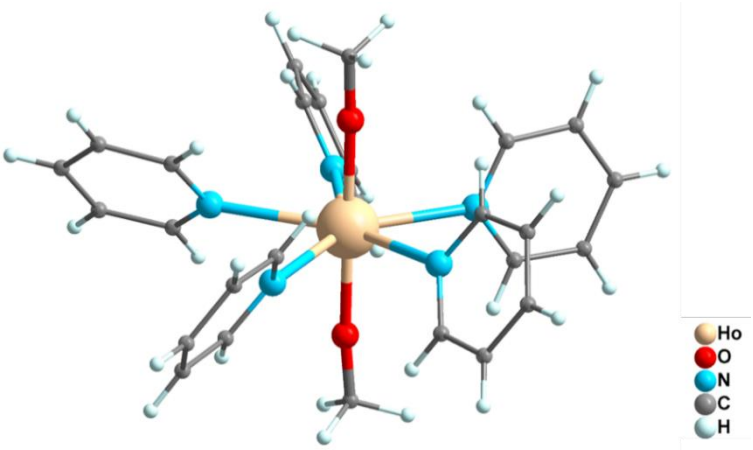

Fig. S37. The model complexes with two OCH_3^- ligands on the axial direction with elongation or contraction of Ho–O bond length. The bond length of Ho–O is sweeping from 1.7 to 2.6 Å by 0.1 Å

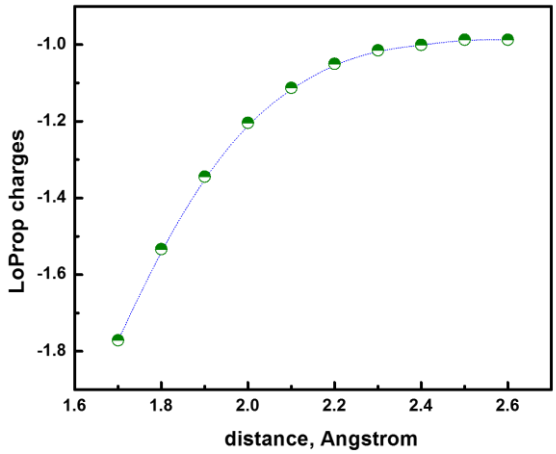

Fig. S38. Correlation with LoProp charges on axial oxygen atoms and Ho–O distance. The green dots represent the result by theoretical calculation based on the model and blue lines are for eye guiding.

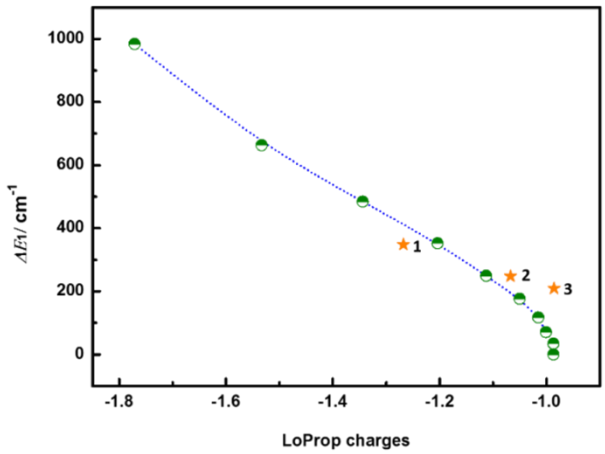

Fig. S39. Correlation with ΔE_1 and LoProp charges on axial oxygen atoms. The green dots represent the result by theoretical calculation based on the model and blue dotted lines are for eye guiding. The orange stars represent the calculation results for complex **1**–**3**.

Table S16. Average transition magnetic moment elements between the states of **1**, given in μ_B^2.

	|+8>	|-8>	|+7>	|-7>	|+6>	|-6>	|+a>	|-a>	|+b>	|-b>	|+c>	|-c>	|+d>	|-d>	|+e>	|-e>	|0>
|+8>	--	3.3E+01	2.1E+00	2.1E+00	1.6E-03	2.2E-03	2.3E-04	1.3E-03	2.7E-03	6.5E-03	5.0E-04	7.0E-04	1.1E-03	9.2E-04	1.3E-03	1.4E-04	4.7E-05
|-8>	3.3E+01	--	2.1E+00	2.1E+00	1.5E-03	1.5E-03	8.3E-04	2.1E-03	7.3E-03	2.8E-03	1.4E-03	2.1E-04	3.5E-04	3.3E-04	6.1E-04	3.3E-05	6.5E-04
|+7>	2.1E+00	2.1E+00	--	2.5E+01	3.4E+00	3.3E+00	2.0E-02	2.7E-01	4.5E-01	1.6E-01	5.4E-02	1.8E-01	1.9E-02	6.3E-02	3.0E-02	3.0E-02	1.1E-03
|-7>	2.1E+00	2.1E+00	2.5E+01	--	3.2E+00	3.5E+00	8.2E-02	1.7E-01	2.4E-01	3.5E-01	1.3E-01	2.0E-01	7.1E-03	9.1E-02	6.7E-03	1.6E-02	3.9E-03
|+6>	1.6E-03	1.5E-03	3.4E+00	3.2E+00	--	1.4E+01	5.7E+00	7.8E-01	3.5E+00	1.4E+00	2.1E+00	9.4E-01	1.0E+00	4.2E-01	1.0E+00	9.1E-02	1.4E-02
|-6>	2.2E-03	1.5E-03	3.3E+00	3.5E+00	1.4E+01	--	5.0E+00	1.0E+00	1.9E-01	3.7E+00	2.5E+00	1.5E+00	6.5E-01	8.1E-01	5.6E-01	4.1E-01	3.5E-01
|+a>	2.3E-04	8.3E-04	2.0E-02	8.2E-02	5.7E+00	5.0E+00	--	1.4E+01	6.9E+00	5.6E-01	1.2E+00	3.1E+00	1.3E-01	5.8E-01	4.5E-01	1.1E-01	7.6E-02
|-a>	1.3E-03	2.1E-03	2.7E-01	1.7E-01	7.8E-01	1.0E+00	1.4E+01	--	7.8E-01	1.2E+01	5.3E+00	7.6E-01	1.1E+00	1.4E+00	4.3E-01	1.9E-02	2.7E-01
|+b>	2.7E-03	7.3E-03	4.5E-01	2.4E-01	3.5E+00	1.9E-01	6.9E+00	7.8E-01	--	1.1E+01	8.0E+00	3.1E+00	2.1E+00	3.7E-01	4.2E-01	2.4E-01	4.0E-01
|-b>	6.5E-03	2.8E-03	1.6E-01	3.5E-01	1.4E+00	3.7E+00	5.6E-01	1.2E+01	1.1E+01	--	1.2E+00	1.1E+00	7.0E-01	1.3E+00	2.6E+00	1.3E+00	1.0E+00
|+c>	5.0E-04	1.4E-03	5.4E-02	1.3E-01	2.1E+00	2.5E+00	1.2E+00	5.3E+00	8.0E+00	1.2E+00	--	6.5E+00	5.6E+00	1.7E+00	9.5E-01	1.3E+00	8.7E-01
|-c>	7.0E-04	2.1E-04	1.8E-01	2.0E-01	9.4E-01	1.5E+00	3.1E+00	7.6E-01	3.1E+00	1.1E+00	6.5E+00	--	1.3E+01	1.2E+00	3.0E+00	6.2E-01	2.3E+00
|+d>	1.1E-03	3.5E-04	1.9E-02	7.1E-03	1.0E+00	6.5E-01	1.3E-01	1.1E+00	2.1E+00	7.0E-01	5.6E+00	1.3E+01	--	7.0E+00	3.5E+00	1.9E+00	7.5E-01
|-d>	9.2E-04	3.3E-04	6.3E-02	9.1E-02	4.2E-01	8.1E-01	5.8E-01	1.4E+00	3.7E-01	1.3E+00	1.7E+00	1.2E+00	7.0E+00	--	1.2E+01	9.7E+00	1.2E+00
|+e>	1.3E-03	6.1E-04	3.0E-02	6.7E-03	1.0E+00	5.6E-01	4.5E-01	4.3E-01	4.2E-01	2.6E+00	9.5E-01	3.0E+00	3.5E+00	1.2E+01	--	2.2E+00	1.1E+01
|-e>	1.4E-04	3.3E-05	3.0E-02	1.6E-02	9.1E-02	4.1E-01	1.1E-01	1.9E-02	2.4E-01	1.3E+00	1.3E+00	6.2E-01	1.9E+00	9.7E+00	2.2E+00	--	2.0E+01
|0>	4.7E-05	6.5E-04	1.1E-03	3.9E-03	1.4E-02	3.5E-01	7.6E-02	2.7E-01	4.0E-01	1.0E+00	8.7E-01	2.3E+00	7.5E-01	1.2E+00	1.1E+01	2.0E+01	--

Table S17. Average transition magnetic moment elements between the states of **2**, given in μ_B^2.

	|+8>	|-8>	|+7>	|-7>	|+6>	|-6>	|+a>	|-a>	|+b>	|-b>	|+c>	|-c>	|+d>	|-d>	|+e>	|-e>	|0>
|+8>	--	3.3E+01	2.2E+00	1.9E+00	5.3E-02	6.6E-02	1.0E-02	4.7E-03	7.1E-03	5.1E-04	4.2E-05	2.1E-05	8.1E-04	1.2E-03	6.5E-04	1.4E-04	2.4E-04
|-8>	3.3E+01	--	1.9E+00	2.2E+00	4.8E-02	7.2E-02	9.9E-03	5.2E-03	5.6E-03	3.5E-04	7.7E-04	1.3E-03	5.4E-04	4.8E-04	6.1E-05	3.3E-04	7.3E-05
|+7>	2.2E+00	1.9E+00	--	2.6E+01	3.0E+00	3.6E+00	4.0E-01	2.7E-01	2.9E-01	1.2E-02	2.8E-03	3.8E-02	7.9E-02	6.0E-02	4.3E-03	1.8E-04	9.6E-04
|-7>	1.9E+00	2.2E+00	2.6E+01	--	3.0E+00	3.7E+00	3.4E-01	2.4E-01	3.3E-01	1.5E-02	1.1E-02	3.0E-03	7.8E-02	9.0E-02	5.0E-03	5.9E-04	3.5E-05
|+6>	5.3E-02	4.8E-02	3.0E+00	3.0E+00	--	1.4E+01	4.4E+00	3.3E+00	2.5E+00	1.7E+00	5.1E-01	2.3E-01	2.4E+00	2.2E+00	3.6E-02	2.2E-02	3.4E-02
|-6>	6.6E-02	7.2E-02	3.6E+00	3.7E+00	1.4E+01	--	2.5E+00	1.0E+00	2.1E+00	1.4E-01	2.4E-01	3.0E-01	4.8E+00	4.7E+00	7.8E-02	2.1E-02	1.3E-02
|+a>	1.0E-02	9.9E-03	4.0E-01	3.4E-01	4.4E+00	2.5E+00	--	1.4E+01	1.1E+01	1.8E+00	9.8E-01	3.3E-02	8.5E-01	1.0E+00	1.2E-01	1.1E-01	3.3E-02
|-a>	4.7E-03	5.2E-03	2.7E-01	2.4E-01	3.3E+00	1.0E+00	1.4E+01	--	1.5E+00	8.2E+00	6.7E+00	1.9E-02	1.2E+00	4.3E-01	2.4E-02	8.7E-02	2.7E-01
|+b>	7.1E-03	5.6E-03	2.9E-01	3.3E-01	2.5E+00	2.1E+00	1.1E+01	1.5E+00	--	8.6E+00	7.2E+00	9.5E-02	1.8E+00	2.2E+00	2.9E-02	1.7E-02	8.0E-02
|-b>	5.1E-04	3.5E-04	1.2E-02	1.5E-02	1.7E+00	1.4E-01	1.8E+00	8.2E+00	8.6E+00	--	1.6E+00	9.3E+00	1.1E+00	3.3E-01	3.5E+00	7.1E-01	3.7E-01
|+c>	4.2E-05	7.7E-04	2.8E-03	1.1E-02	5.1E-01	2.4E-01	9.8E-01	6.7E+00	7.2E+00	1.6E+00	--	1.3E+01	3.2E-01	5.1E-01	5.1E+00	1.1E+00	1.8E-01
|-c>	2.1E-05	1.3E-03	3.8E-02	3.0E-03	2.3E-01	3.0E-01	3.3E-02	1.9E-02	9.5E-02	9.3E+00	1.3E+01	--	2.5E+00	9.8E-01	4.0E+00	1.8E+00	5.1E+00
|+d>	8.1E-04	5.4E-04	7.9E-02	7.8E-02	2.4E+00	4.8E+00	8.5E-01	1.2E+00	1.8E+00	1.1E+00	3.2E-01	2.5E+00	--	1.0E+01	4.0E+00	4.9E+00	3.3E+00
|-d>	1.2E-03	4.8E-04	6.0E-02	9.0E-02	2.2E+00	4.7E+00	1.0E+00	4.3E-01	2.2E+00	3.3E-01	5.1E-01	9.8E-01	1.0E+01	--	6.4E+00	5.3E+00	3.1E+00
|+e>	6.5E-04	6.1E-05	4.3E-03	5.0E-03	3.6E-02	7.8E-02	1.2E-01	2.4E-02	2.9E-02	3.5E+00	5.1E+00	4.0E+00	4.0E+00	6.4E+00	--	6.3E+00	7.9E+00
|-e>	1.4E-04	3.3E-04	1.8E-04	5.9E-04	2.2E-02	2.1E-02	1.1E-01	8.7E-02	1.7E-02	7.1E-01	1.1E+00	1.8E+00	4.9E+00	5.3E+00	6.3E+00	--	1.7E+01
|0 >	2.4E-04	7.3E-05	9.6E-04	3.5E-05	3.4E-02	1.3E-02	3.3E-02	2.7E-01	8.0E-02	3.7E-01	1.8E-01	5.1E+00	3.3E+00	3.1E+00	7.9E+00	1.7E+01	--

Table S18. Average transition magnetic moment elements between the states of **3**, given in μ_B^2.

	|+8>	|-8>	|+7>	|-7>	|+6>	|-6>	|+a>	|-a>	|+b>	|-b>	|+c>	|-c>	|+d>	|-d>	|+e>	|-e>	|0>
|+8>	--	3.3E+01	2.0E+00	2.2E+00	1.5E-04	5.8E-03	3.6E-03	5.0E-04	1.0E-02	1.1E-02	8.9E-03	5.9E-04	1.1E-02	2.6E-03	9.9E-04	1.0E-04	9.6E-03
|-8>	3.3E+01	--	2.1E+00	2.0E+00	4.5E-03	9.4E-03	2.5E-03	4.8E-04	1.1E-02	1.6E-02	6.5E-06	6.1E-03	1.4E-03	8.5E-06	1.6E-02	4.4E-03	2.2E-04
|+7>	2.0E+00	2.1E+00	--	2.5E+01	8.4E-01	1.1E-02	5.8E-01	2.7E-01	2.4E+00	3.0E+00	4.5E-01	4.6E-01	2.2E-02	5.5E-03	1.4E-02	3.4E-02	1.9E-02
|-7>	2.2E+00	2.0E+00	2.5E+01	--	5.3E-01	1.1E-01	3.6E-01	2.0E-01	3.2E+00	3.1E+00	2.0E-01	2.9E-01	5.2E-03	7.6E-02	1.2E-02	1.8E-03	3.6E-02
|+6>	1.5E-04	4.5E-03	8.4E-01	5.3E-01	--	2.3E+01	1.0E+01	7.0E-03	2.3E+00	4.9E-03	2.5E-02	1.2E+00	2.1E-02	3.8E-03	4.0E-02	2.9E-02	4.9E-03
|-6>	5.8E-03	9.4E-03	1.1E-02	1.1E-01	2.3E+01	--	5.2E-01	3.4E+00	1.6E+00	2.7E+00	5.8E+00	9.0E-02	2.4E-04	3.5E-03	4.1E-01	1.5E-01	1.2E-01
|+a>	3.6E-03	2.5E-03	5.8E-01	3.6E-01	1.0E+01	5.2E-01	--	1.7E+01	2.5E-01	6.6E-01	6.6E+00	2.2E-02	4.2E-01	2.5E-01	4.1E-02	4.9E-01	3.1E-01
|-a>	5.0E-04	4.8E-04	2.7E-01	2.0E-01	7.0E-03	3.4E+00	1.7E+01	--	5.7E+00	2.7E-02	8.2E-01	5.2E+00	1.8E-02	3.6E+00	1.4E-01	9.7E-01	3.7E-02
|+b>	1.0E-02	1.1E-02	2.4E+00	3.2E+00	2.3E+00	1.6E+00	2.5E-01	5.7E+00	--	1.2E+01	1.0E+00	9.7E-01	3.9E+00	2.4E-01	3.0E+00	4.7E-01	6.5E-01
|-b>	1.1E-02	1.6E-02	3.0E+00	3.1E+00	4.9E-03	2.7E+00	6.6E-01	2.7E-02	1.2E+01	--	3.6E+00	1.8E+00	5.7E+00	5.0E-02	4.8E+00	9.4E-02	3.6E-02
|+c>	8.9E-03	6.5E-06	4.5E-01	2.0E-01	2.5E-02	5.8E+00	6.6E+00	8.2E-01	1.0E+00	3.6E+00	--	1.3E+01	9.5E-01	3.8E+00	5.3E-01	6.5E-02	9.0E-01
|-c>	5.9E-04	6.1E-03	4.6E-01	2.9E-01	1.2E+00	9.0E-02	2.2E-02	5.2E+00	9.7E-01	1.8E+00	1.3E+01	--	3.4E+00	3.6E+00	2.4E+00	2.7E+00	2.7E+00
|+d>	1.1E-02	1.4E-03	2.2E-02	5.2E-03	2.1E-02	2.4E-04	4.2E-01	1.8E-02	3.9E+00	5.7E+00	9.5E-01	3.4E+00	--	4.8E-02	9.2E+00	1.9E+00	1.2E+01
|-d>	2.6E-03	8.5E-06	5.5E-03	7.6E-02	3.8E-03	3.5E-03	2.5E-01	3.6E+00	2.4E-01	5.0E-02	3.8E+00	3.6E+00	4.8E-02	--	1.9E+00	1.8E+01	5.8E+00
|+e>	9.9E-04	1.6E-02	1.4E-02	1.2E-02	4.0E-02	4.1E-01	4.1E-02	1.4E-01	3.0E+00	4.8E+00	5.3E-01	2.4E+00	9.2E+00	1.9E+00	--	6.3E+00	8.7E+00
|-e>	1.0E-04	4.4E-03	3.4E-02	1.8E-03	2.9E-02	1.5E-01	4.9E-01	9.7E-01	4.7E-01	9.4E-02	6.5E-02	2.7E+00	1.9E+00	1.8E+01	6.3E+00	--	6.3E+00
|0>	9.6E-03	2.2E-04	1.9E-02	3.6E-02	4.9E-03	1.2E-01	3.1E-01	3.7E-02	6.5E-01	3.6E-02	9.0E-01	2.7E+00	1.2E+01	5.8E+00	8.7E+00	6.3E+00	--

References

1. F. Aquilante, J. Autschbach, R. K. Carlson, L. F. Chibotaru, M. G. Delcey, L. De Vico, I. Fdez. Galván, N. Ferré, L. M. Frutos, L. Gagliardi, M. Garavelli, A. Giussani, C. E. Hoyer, G. Li Manni, H. Lischka, D. Ma, P. Å. Malmqvist, T. Müller, A. Nenov, M. Olivucci, T. B. Pedersen, D. Peng, F. Plasser, B. Pritchard, M. Reiher, I. Rivalta, I. Schapiro, J. Segarra-Martí, M. Stenrup, D. G. Truhlar, L. Ungur, A. Valentini, S. Vancoillie, V. Veryazov, V. P. Vysotskiy, O. Weingart, F. Zapata and R. Lindh, *J. Comput. Chem.*, 2016, **37**, 506–541.
2. B. O. Roos, R. Lindh, P.-Å. Malmqvist, V. Veryazov and P.-O. Widmark, *J. Phys. Chem. A*, 2004, **108**, 2851–2858.
3. C. A. Goodwin, F. Ortu, D. Reta, N. F. Chilton, D. P. Mills, *Nature*, 2017, **548**, 439-442;
4. P. A. Malmqvist, B. O. Roos, B. Schimmelpfennig. *Chem. Phys. Lett*., 2002, **357**, 230−240.
5. B. O. Roos, R. Lindh, P.-Å. Malmqvist, V. Veryazov and P.-O. Widmark, *Chem. Phys. Lett*., 2005, **409**, 295–299.